2
Theory of Infrared Absorption and Raman Spectroscopy

Molecular vibrations can be excited via two physical mechanisms: the absorption of light quanta and the inelastic scattering of photons (Fig. 2.1) (Herzberg 1945). Direct absorption of photons is achieved by irradiation of molecules with poly-chromatic light that includes photons of energy matching the energy difference $h\nu_k$ between two vibrational energy levels, the initial (i, e.g., ground state) and the final (f, e.g., first excited state) vibrational state.

$$h\nu_k = h\nu_f - h\nu_i \tag{2.1}$$

As these energy differences are in the order of 0.5 and 0.005 eV, light with wavelengths longer than 2.5 μm, that is infrared (IR) light, is sufficient to induce the vibrational transitions. Thus, vibrational spectroscopy that is based on the direct absorption of light quanta is denoted as IR absorption or IR spectroscopy.

The physical basis of IR light absorption is very similar to light absorption in the ultraviolet (UV)–visible (vis) range, which causes electronic transitions or combined electronic–vibrational (vibronic) transitions. Thus, UV–vis absorption spectroscopy can, in principle, also provide information about molecular vibrations. However, for molecules in the condensed phase at ambient temperature, the vibrational fine structure of the absorption spectra is only poorly resolved , if at all, such that vibrational spectroscopy of biomolecules by light absorption is restricted to the IR range.
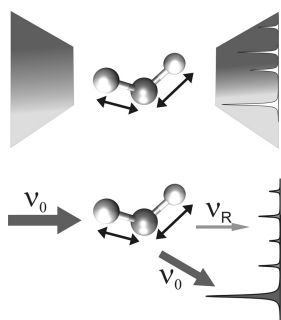

Fig. 2.1 Illustration of the excitation of molecular vibrations in IR (top) and Raman (bottom) spectroscopy. In IR spectroscopy, the vibrational transitions are induced by absorption of light quanta from a continuous light source in the IR spectral region. Vibrational Raman transitions correspond to inelastic scattering (ν_R; thin arrow) of the incident monochromatic light (ν_0) whereas the elastic scattering (ν_0) is represented by the thick arrow.

In contrast to IR spectroscopy, the scattering mechanism for exciting molecular vibrations requires monochromatic irradiation. A portion of the incident photons is scattered inelastically such that the energy of the scattered photons ($h\nu_R$) differs from that of the incident photons ($h\nu_0$). According to the law of conversation of energy, the energy difference corresponds to the energy change of the molecule, which refers to the transition between two vibrational states. Thus, the energy differences

$$h\nu_0 - h\nu_R = h\nu_f - h\nu_i \tag{2.2}$$

lie in the same range as the transitions probed by the direct absorption of mid-IR quanta, although photons of UV, visible, or near-infrared light are used to induce scattering. This inelastic scattering of photons was first discovered by the Indian scientist C. V. Raman in 1928 and is thus denoted as the Raman effect.

Vibrational transitions may be associated with rotational transitions that can only be resolved in high resolution spectra of molecules in the gas phase and is, therefore, not relevant for the vibrational spectroscopy of biomolecules. Thus, vibration–rotation spectra will not be treated in this book.

Depending on the molecule, the same or different vibrational transitions are probed in IR and Raman spectroscopy and both techniques provide complementary information in many instances. Hence, IR and Raman spectra are usually plotted in an analogous way to facilitate comparison. The ordinate refers to the extent of the absorbed (IR) or scattered (Raman) light. In IR absorption spectroscopy, the amount of absorbed light is expressed in units of absorbance or, albeit physically less correct but frequently used, in terms of the optical density. In contrast, Raman intensities are measured in terms of counts per second, i.e., of photons detected per second. As this value depends on many apparatus-specific parameters, in most instances only relative intensities represent physically meaningful quantities. Thus, the Raman intensity scale is typically expressed in terms of arbitrary units or the scale is even omitted. The energy of the vibrational transition, expressed in terms of wavenumbers (cm^{-1}), is given on the abscissa, corresponding to the frequency of the absorbed light ν_{abs} in IR spectroscopy and to the frequency difference between the exciting and scattered light, $\nu_0 - \nu_R$, in Raman spectroscopy.

The principle sources of information in vibrational spectroscopy are the energies of the vibrational transitions and the strength of their interaction with the IR or UV–vis radiation, i.e., the band intensities. Classical mechanics constitutes the basis for describing the relationship between vibrational frequencies and the molecular structure and force fields whereas quantum mechanics is indispensable for understanding the transition probabilities and thus the intensities of vibrational bands in the IR or Raman spectra.

2.1
Molecular Vibrations

As the starting point for introducing the concept of harmonic vibrations, it is instructive to consider molecules as an array of point masses that are connected

with each other by mass-less springs representing the intramolecular interactions between the atoms (Wilson et al. 1955). The simplest case is given by two masses, m_A and m_B, corresponding to a diatomic molecule A–B. Upon displacement of the spheres along the x-axis from the equilibrium position by Δx, a restoring force F_x acts on the spheres, which according to Hooke's law, is given by

$$F_x = -f\Delta x \tag{2.3}$$

Here f is the spring or force constant, which is a measure of the rigidity of the spring, that is, the strength of the bond. The potential energy V then depends on the square of the displacement from the equilibrium position

$$V = \frac{1}{2}f\Delta x^2 \tag{2.4}$$

For the kinetic energy T of the oscillating motion one obtains

$$T = \frac{1}{2}\mu(\Delta\dot{x})^2 \tag{2.5}$$

where μ is the reduced mass defined by

$$\mu = \frac{m_A \cdot m_B}{m_A + m_B} \tag{2.6}$$

Because of the conservation of energy, the sum of V and T must be constant, such that the sum of the first derivatives of V and T is equal to zero, as expressed by Eq. (2.7):

$$0 = \frac{dT}{dt} + \frac{dV}{dt} = \frac{1}{2}\frac{d(\Delta\dot{x}^2)}{dt} + \frac{1}{2}f\frac{d(\Delta x^2)}{dt} \tag{2.7}$$

which eventually leads to the Newton equation of motion

$$\frac{d^2\Delta x}{dt^2} + \frac{f}{\mu}\Delta x = 0 \tag{2.8}$$

Equation (2.8) represents the differential equation for a harmonic motion with the solution given by a sine or cosine function, i.e.,

$$\Delta x = A \cdot \cos(\omega t + \varphi) \tag{2.9}$$

where A, ω, and φ are the amplitude, circular frequency, and phase, respectively. Combining Eq. (2.9) with its second derivative one obtains

$$\frac{d^2\Delta x}{dt^2} + \omega^2\Delta x = 0 \tag{2.10}$$

such that comparison with Eq. (2.8) yields

$$\omega = \sqrt{\frac{f}{\mu}} \qquad (2.11)$$

Equation (2.11) describes what one intuitively expects: the circular frequency of the harmonic vibration increases when the rigidity of the spring (or the strength of the bond) increases but decreases with increasing masses of the spheres. In order to express the circular frequency in wavenumbers (in cm^{-1}), Eq. (2.11) has to be divided by $2\pi c$ (with c given in cm s^{-1}):

$$\tilde{\nu} = \frac{1}{2\pi c} \sqrt{\frac{f}{\mu}} \qquad (2.12)$$

In contrast to the straightforward treatment of a two-body system, including a third sphere corresponding to a triatomic molecule clearly represents a conceptual challenge (Wilson et al. 1955). Let us consider a bent molecule such as H_2O as an example (Fig. 2.2). Following the same strategy as for the diatomic molecule, we analyse the displacements of the individual atoms in terms of the restoring forces. There are two questions to be answered. (a) What are the displacements that lead to vibrations? (b) Are all possible displacements allowed?

In the Cartesian coordinate system, each atom can be displaced in the x-, y-, and z-directions, corresponding to three degrees of freedom. Thus, a molecule of N atoms (α) has in total $3N$ degrees of freedom, but not all of them correspond to vibrational degrees of freedom. If all atoms are displaced in the x-, y-, and z-directions by the same increments, the entire molecule moves in a certain direction, representing one of the three translational degrees of freedom. Furthermore, one can imagine displacements of the atoms that correspond to the rotation of
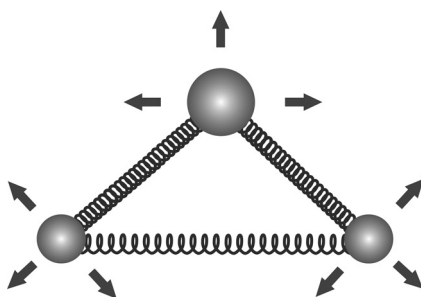

Fig. 2.2 Illustration of the vibrating H_2O molecule represented by spheres that are connected via springs of different strengths. The tighter springs linking the large sphere (oxygen) with each of the small spheres (hydrogen) symbolises the chemical bonds between two atoms, whereas the looser spring refers to weaker interactions between two atoms that are not connected via a chemical bond.

the molecule. It can easily be seen that a nonlinear molecule (i.e., where the atoms are not located along a straight line) has three rotational degrees of freedom, whereas there are only two for a linear molecule. Thus, the remaining $3N - 6$ and $3N - 5$ degrees of freedom correspond to the vibrations of a nonlinear and a linear molecule, respectively. For the treatment of molecular vibrations in terms of Cartesian coordinates, the rotational and translational degrees of freedom can be separated by choosing a rotating coordinate system with its origin in the centre of mass of the molecule.

As an important implication of these considerations, we note that the vibrational degrees of freedom and thus the number of molecular vibrations are uniquely determined by the number of atoms in the molecule. In our example of a nonlinear three-atomic molecule there are just $3 \ (= 3 \cdot 3 - 6)$ vibrational degrees of freedom. Thus, molecular vibrations do not represent random motions but well-defined displacements of the individual atoms. Consequently, one may intuitively expect that these vibrations, which are denoted as normal modes, are characteristic of a given molecule. The primary task of the normal mode analysis is to decode the relationships between normal modes, specifically their frequencies, and molecular properties.

2.1.1
Normal Modes

To determine the normal mode frequencies, we begin by expressing the kinetic and potential energy in terms of the displacements of the Cartesian coordinates for each atom α (Wilson et al. 1955). For the kinetic energy one obtains [see Eq. (2.5)]

$$T = \frac{1}{2} \sum_{\alpha=1}^{N} m_\alpha \left[\left(\frac{d\Delta x_\alpha}{dt} \right)^2 + \left(\frac{d\Delta y_\alpha}{dt} \right)^2 + \left(\frac{d\Delta z_\alpha}{dt} \right)^2 \right] \tag{2.13}$$

At this point it is convenient to introduce so-called mass-weighted Cartesian displacement coordinates, which are defined according to

$$q_1 = \sqrt{m_1}\Delta x_1, \quad q_2 = \sqrt{m_1}\Delta y_1, \quad q_3 = \sqrt{m_1}\Delta z_1 \quad \text{for atom } \alpha = 1$$
$$q_4 = \sqrt{m_2}\Delta x_2, \quad q_5 = \sqrt{m_2}\Delta y_2, \quad q_6 = \sqrt{m_2}\Delta z_2 \quad \text{for atom } \alpha = 2 \tag{2.14}$$

and correspondingly for all other atoms such that one obtains $3N$ mass-weighted Cartesian displacement coordinates. Substituting Eq. (2.14) in Eq. (2.13) simplifies the expression for the kinetic energy to

$$T = \frac{1}{2} \sum_{i=1}^{3N} \dot{q}_i^2 \tag{2.15}$$

To derive the appropriate expression for the potential energy, V, is more complicated as it has to take into account all possible interactions between the

individual atoms, which primarily include the bonding interactions but also non-bonding (electrostatic, van-der-Waals) interactions. For the three-atomic water molecule in Fig. 2.2 this implies that the displacement of one hydrogen atom depends on the attractive and repulsive forces of both the central oxygen and the second hydrogen atom. Within the framework of the sphere–spring model we therefore also have to connect both hydrogen "spheres" via a spring which, however, is less rigid than those connecting the hydrogen spheres with the oxygen.

It is convenient to expand the potential energy in a Taylor series in terms of the displacement coordinates Δx_i, Δy_i, Δz_i, which can be also expressed in terms of the coordinates q_i defined in Eq. (2.14).

$$V = V_0 + \sum_{i=1}^{3N} \left(\frac{\partial V}{\partial q_i}\right)_0 q_i + \frac{1}{2} \sum_{i,j=1}^{3N} \left(\frac{\partial^2 V}{\partial q_i \partial q_j}\right)_0 q_i q_j + \cdots \cdots \tag{2.16}$$

The first term refers to the potential energy at equilibrium, which we can set equal to zero as we are interested in changes to V brought about by displacements of the individual atoms. At equilibrium, infinitesimal changes in q_i do not cause a change in V, such that the second term is also zero. For small displacements q_i within the harmonic approximation, higher order terms can be neglected, such that Eq. (2.16) is simplified to

$$V \cong \frac{1}{2} \sum_{i,j=1}^{3N} \left(\frac{\partial^2 V}{\partial q_i \partial q_j}\right)_0 = \frac{1}{2} \sum_{i,j=1}^{3N} f_{ij} q_i q_j \tag{2.17}$$

where f_{ij} are the force constants.

In books on classical mechanics it is shown that, in the absence of external and non-conservative forces, Newton's equations of motion can be written in the following form:

$$\frac{\mathrm{d}}{\mathrm{d}t} \frac{\partial T}{\partial \dot{q}_j} + \frac{\partial V}{\partial q_j} = 0 \tag{2.18}$$

which yields

$$\ddot{q}_j + \sum_{i=1}^{3N} f_{ij} q_i = 0 \tag{2.19}$$

Equation (2.19) is equivalent to Eq. (2.10) for the diatomic harmonic oscillator, except that it represents not just one but a set of $3N$ linear second-order differential equations for which we can write the general solution, in analogy to Eq. (2.9),

$$q_i = A_i \cos(\sqrt{\lambda} t + \varphi) \tag{2.20}$$

Inserting Eq. (2.20) into Eq. (2.19) yields

$$-A_j\lambda + \sum_{i=1}^{3N} f_{ij}A_i = 0 \tag{2.21}$$

which corresponds to $3N$ linear equations for A_j. These equations only have a solution different from zero if the $3N \cdot 3N$ determinant vanishes (secular equation):

$$\begin{vmatrix} f_{11} - \lambda & f_{12} & f_{13} & \cdots\cdots & f_{1,3N} \\ f_{21} & f_{22} - \lambda & f_{23} & \cdots\cdots & f_{2,3N} \\ f_{31} & f_{32} & f_{33} - \lambda & \cdots\cdots & f_{3,3N} \\ \cdots\cdots & \cdots\cdots & \cdots\cdots & \cdots\cdots & \cdots\cdots \\ f_{3N,1} & f_{3N,2} & f_{3N,3} & \cdots\cdots & f_{3N,3N} - \lambda \end{vmatrix} = 0 \tag{2.22}$$

There are $3N$ solutions for λ corresponding to $3N$ frequencies $\lambda^{1/2}$. As the summation has been made over all $3N$ degrees of freedom, 6 (5) of these solutions refer to translational and rotational motions of the nonlinear (linear) molecules and, therefore, must be zero. Thus, Eq. (2.22) yields only $3N - 6$ ($3N - 5$) non-zero values for λ. The proof for this is lengthy and is not shown here (Wilson et al. 1955). The non-zero solutions correspond to the so-called normal modes.

Once the individual λ_k values have been determined, the amplitudes A_i for each normal mode have to be determined on the basis of in Eq. (2.21).

$$(f_{11} - \lambda_k)A_{1k} + f_{12}A_{2k} + \cdots\cdots + f_{1,3N}A_{3N,k} = 0$$

$$f_{21}A_{1k} + (f_{22} - \lambda_k)A_{2k} + \cdots\cdots + f_{2,3N}A_{3N,k} = 0$$

$$\cdots\cdots\cdots\cdots\cdots\cdots\cdots\cdots\cdots\cdots\cdots\cdots\cdots\cdots\cdots\cdots \tag{2.23}$$

$$f_{3N,1}A_{1k} + f_{3N,2} + \cdots\cdots + (f_{3N,3N} - \lambda_k)A_{3N,k} = 0$$

As Eq. (2.23) represents a set of homogeneous equations, only relative amplitudes can be obtained and a normalisation is required, as will be discussed below. The amplitudes A_{ik} describe the character of a normal mode as they quantify the displacements of each atom i in each normal mode k. Eqs. (2.20 and 2.23) imply that in a given normal mode k all atoms vibrate in-phase and with the same frequency $(\lambda_k)^{1/2}$, but with different amplitudes. Thus, it is always an approximation, albeit a useful one in many instances, to characterise normal modes of polyatomic molecules in terms of specific group vibrations, i.e., if only one coordinate dominates the normal mode.

Although the treatment of normal modes in the Cartesian coordinate system is straightforward, it has the disadvantage of distributing all information for a given normal mode among $3N$ equations. In particular, for describing probabilities of vibrational transitions [see Eq. (2.2)] a more compact presentation is desirable. For this purpose, the mass-weighted Cartesian coordinates q_i are converted into normal coordinates Q_k via an orthogonal transformation according to

$$Q_k = \sum_{i=1}^{3N} l_{ik} q_i \tag{2.24}$$

The transformation coefficients l_{ik} are chosen such that T and V, expressed as a function of Q_k, adopt the same form as Eqs. (2.15 and 2.16) and the potential energy does not depend on cross products $Q_k \cdot Q_{k'}$ (with $k \neq k'$). The solution of Newton's equation of motion thus leads to

$$Q_k = K_k \cos(\sqrt{\lambda_k} t + \varphi_k) \tag{2.25}$$

with arbitrary values of K_k and φ_k. The representation of molecular vibrations in normal coordinates is particularly important for the quantum mechanical treatment of the harmonic oscillator (Box 2A).

2.1.2
Internal Coordinates

The normal coordinate system is, mathematically, a very convenient system and, moreover, is required for the quantum chemical treatment of vibrational transitions. However, it is not a very illustrative system as molecular vibrations are usually imagined in terms of stretching or bending motions of molecules or parts of molecules. Such motions cannot be intuitively deduced from a normal coordinate or the array of mass-weighted Cartesian coordinates (Wilson et al. 1955). It is, therefore, desirable to introduce a coordinate system that is based on ''structural elements'' of molecules, such as bond lengths and angles, and torsional and out-of-plane angles. These so-called internal coordinates are derived from Cartesian displacement coordinates $(\Delta x_\alpha, \Delta y_\alpha, \Delta z_\alpha)$ on the basis of the geometry of the molecule.

The displacement of each atom α is defined by the vector $\vec{\rho}_\alpha(\Delta x_\alpha, \Delta y_\alpha, \Delta z_\alpha)$, which is related to the internal coordinate S_t according to

$$S_t = \sum_{\alpha=1}^{N} \vec{s}_{t\alpha} \cdot \vec{\rho}_\alpha \tag{2.26}$$

The vector $\vec{s}_{t\alpha}$ is chosen such that it points in the direction of the largest displacement of $\vec{\rho}_\alpha$ corresponding to the greatest increase in S_t. This statement is best illustrated on the basis of the most simple internal coordinate, the bond stretching coordinate (Fig. 2.3). A stretching coordinate is defined by two atoms ($\alpha = 1, 2$). Thus, for this coordinate the displacement of all other atoms is zero and the sum in Eq. (2.26) only refers to two terms. The largest displacement from the equilibrium positions occur along the axis of the bond assumed to be the x-axis but in opposite directions for atom 1 and 2. Expressing $\vec{s}_{t1}$ and $\vec{s}_{t2}$ in terms of unit vectors we thus obtain

$$\vec{s}_{t1} = \vec{e}_{21} = -\vec{e}_{12} \quad \text{and} \quad \vec{s}_{t2} = \vec{e}_{12} \tag{2.27}$$
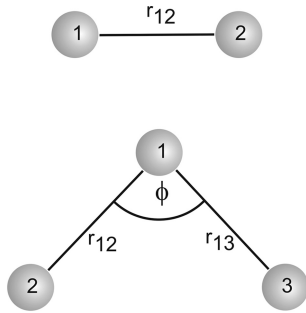
Fig. 2.3 Definition of internal coordinates: top, stretching coordinate; and bottom, bending coordinate.

According to Eq. (2.26), the bond stretching coordinate S_s is then given by

$$S_s = \Delta x_1 - \Delta x_2 \tag{2.28}$$

For the valence angle bending coordinate S_b we have to consider three atoms (Fig. 2.3). To achieve the largest contribution to S_b, the displacements of atoms 1 and 2 and thus $\vec{s}_{t1}$ and $\vec{s}_{t2}$ are perpendicular to the vectors defining the respective bonds between the atoms 1 and 3 and 2 and 3. A unit (infinitesimal) displacement of atom 1 along $\vec{s}_{t1}$ increases ϕ by the amount of $1/r_{31}$. Geometric considerations then yield

$$\vec{s}_{t1} = \frac{\vec{e}_{31} \cdot \cos \phi - \vec{e}_{32}}{r_{31} \cdot \sin \phi} \tag{2.29}$$

and analogous expressions can be derived for $\vec{s}_{t2}$ and $\vec{s}_{t3}$.

$$\vec{s}_{t2} = \frac{\vec{e}_{32} \cdot \cos \phi - \vec{e}_{31}}{r_{32} \cdot \sin \phi} \tag{2.30}$$

$$\vec{s}_{t3} = \frac{[(r_{31} - r_{32} \cos \phi)\vec{e}_{31} + (r_{32} - r_{31} \cos \phi)\vec{e}_{32}]}{r_{31} r_{32} \sin \phi} \tag{2.31}$$

Insertion of the Eqs. (2.29, 2.30, and 2.31) into Eq. (2.26) yields the internal coordinate for the bending motion.

Further internal coordinates are the out-of-plane deformation and torsional coordinates that refer to the angle between a bond and a plane and to a dihedral angle, respectively. In both instances, four atoms are required to define these coordinates (Wilson et al. 1955).

2.1.3
The *FG*-Matrix

For a molecule with $3N - 6$ vibrational degrees of freedom, a complete set of internal coordinates includes $3N - 6$ independent internal coordinates. The defini-

tion of this set is straightforward for small molecules such as the triatomic non-linear molecule in Fig. 2.2, for which two bond stretching and one bond angle deformation coordinates are necessary and sufficient. However, with the increasing size of the molecules, definition of the coordinate set becomes more and more complicated. Thus, it is of particular importance to choose systematic strategies for selection of the internal coordinates. Appropriate protocols have been proposed in the literature, however, sorting out independent and dependent internal coordinates may represent a challenge in many instances (Wilson et al. 1955; Fogarasi et al. 1992). Such redundancies appear in particular in ring systems and have to be removed by appropriate boundary conditions *a posteriori*.

The internal coordinates are independent of the masses of the atoms involved, which are introduced by setting up the so-called *G*-matrix, which is derived in Wilson et al. (1955). The elements of the *G*-matrix are given by

$$G_{tt'} = \sum_{\alpha=1}^{N} \mu_\alpha \vec{s}_{t\alpha} \cdot \vec{s}_{t'\alpha} \qquad (2.32)$$

where μ_α is the reciprocal mass of atom α.

The *G*-matrix now contains all the information on the chemical constitution and the structure of the molecule. The elements $G_{tt'}$ represent a $t \cdot t'$ matrix with the number of internal coordinates t being equal to the number of vibrational degrees of freedom. For a nonlinear three-atomic molecule (Fig. 2.2) the *G*-matrix can be easily calculated using Eq. (2.32) on the basis of the $\vec{s}_{t1}$ vectors defined in Eqs. (2.27–2.31).

$$\begin{vmatrix} \mu_1 + \mu_2 & \mu_3 \cos \phi & \dfrac{-\mu_3 \sin \phi}{r_{32}} \\[2mm] \mu_3 \cos \phi & \mu_2 + \mu_3 & \dfrac{-\mu_3 \sin \phi}{r_{31}} \\[2mm] \dfrac{-\mu_3 \sin \phi}{r_{32}} & \dfrac{-\mu_3 \sin \phi}{r_{31}} & \dfrac{\mu_1}{r_{31}^2} + \dfrac{\mu_2}{r_{32}^2} - \mu_3 \left(\dfrac{1}{r_{31}^2} + \dfrac{1}{r_{32}^2} - \dfrac{2 \cos \phi}{r_{31} r_{32}} \right) \end{vmatrix} = G \qquad (2.33)$$

In analogy to the treatment in the Cartesian and normal coordinate systems, the next step is to derive expressions for the kinetic and potential energy in terms of the internal coordinates (Wilson et al. 1955). The kinetic energy in terms of internal coordinates is given by

$$T = \frac{1}{2} \sum_{tt'} (G^{-1})_{tt'} \dot{S}_t \dot{S}_{t'} \qquad (2.34)$$

where $(G^{-1})_{tt'}$ are the elements of the inverse *G*-matrix [Eq. (2.33)]. The expression for the potential energy is written as

$$V = \frac{1}{2} \sum_{tt'} F_{tt'} S_t S_{t'} \qquad (2.35)$$

The Newton equation of motion then adopts a form similar to Eq. (2.19), with the solution for the differential equation given by

$$s_t = A_t \cos(\sqrt{\lambda}\, t + \varphi) \tag{2.36}$$

in analogy to Eq. (2.20). Thus, one obtains the secular equation

$$
\begin{vmatrix}
F_{11} - (G^{-1})_{11}\lambda & F_{12} - (G^{-1})_{12}\lambda & F_{13} - (G^{-1})_{13}\lambda & \cdots\cdots & F_{1n} - (G^{-1})_{1n}\lambda \\
F_{21} - (G^{-1})_{21}\lambda & F_{22} - (G^{-1})_{22}\lambda & F_{23} - (G^{-1})_{23}\lambda & \cdots\cdots & F_{2n} - (G^{-1})_{2n}\lambda \\
F_{31} - (G^{-1})_{31}\lambda & F_{32} - (G^{-1})_{32}\lambda & F_{33} - (G^{-1})_{33}\lambda & \cdots\cdots & F_{3n} - (G^{-1})_{3n}\lambda \\
\cdots\cdots & \cdots\cdots & \cdots\cdots & \cdots\cdots & \cdots\cdots \\
F_{n1} - (G^{-1})_{n1}\lambda & F_{n2} - (G^{-1})_{n2}\lambda & F_{n3} - (G^{-1})_{n3}\lambda & \cdots\cdots & F_{nn} - (G^{-1})_{nn}\lambda
\end{vmatrix} = 0
$$
$$\tag{2.37}$$

which can be expressed in a much simpler way through matrix formalism

$$|F - G^{-1}\lambda| = 0 \tag{2.38}$$

Equation (2.38) is the so-called *FG*-matrix, which upon applying matrix algebra can be re-written in various forms (Wilson et al. 1955).

The secular equations in Eq. (2.37) have t solutions for λ from which the "frequencies" (in wavenumbers) are obtained according to

$$\tilde{\nu} = \frac{1}{2\pi c} \sqrt{\lambda} \tag{2.39}$$

Once the eigenvalues λ_k have been evaluated, the nature of the normal mode has to be determined by evaluating the relative amplitudes A_{tk}. Using Eq. (2.35), these quantities can be normalised with respect to the potential energy such that the relative contributions of each internal coordinate t to all normal modes and the relative contributions of all internal coordinates in each normal mode sum up to one. This procedure allows for an illustrative description of the character of the normal modes in terms of the potential energy distribution (PED, given in %), e.g., $x\%$ of the stretching coordinate t_1, $\gamma\%$ of the bending coordinate t_2, etc.

Both the *G*- and the *F*-matrix are symmetric, that is $G_{tt'} = G_{t't}$ and $F_{tt'} = F_{t't}$. This corresponds to $1/2[v(v + 1)]$ different $G_{tt'}$ and $F_{tt'}$ elements for a molecule with v vibrational degrees of freedom. Whereas the $G_{tt'}$ elements can be computed readily when the structure of the molecule is known, the $F_{tt'}$ elements are not known *a priori*. Even for a simple three-atomic nonlinear molecule as depicted in Fig. 2.2, there are six different force constants: the stretching force constants F_{11} and F_{22}, referring to the bonds between the atoms 1 and 2 and the atoms 2 and 3, respectively, the bending force constant F_{33}, and the three interaction force constants F_{12}, F_{13}, and F_{23}, which are related to the interactions between the individual stretching and bending coordinates. On the other hand,

there are only three normal mode frequencies that can be determined experimentally. This example illustrates the inherent problem of empirical vibrational analysis: the number of observables is always much smaller than the number of unknown force constants.

In some instances, it is possible to utilise the symmetry properties of normal modes (Box 2B) (Wilson et al. 1955; Cotton 1990). For symmetric molecules the normal modes can be classified in terms of the symmetry species of the point group to which the molecule belongs. Each point group is characterised by a set of symmetry operations, such as the reflection in a mirror plane or an *n*-fold rotation about an *n*-fold axis of symmetry. Now the individual normal modes are either symmetric or antisymmetric to these operations. For instance, a normal mode that is symmetric to all symmetry operations of the point group is denoted as a totally symmetric mode and thus belongs to the totally symmetric species of the point group. On the basis of group theory, it is possible to determine the number of normal modes for each symmetry species of the point group. This does not just facilitate computing the normal mode frequencies, because the secular determinant can be factorised. Moreover, one may predict IR and Raman activity of the individual modes taking into account the symmetry properties of the dipole moment and polarisability operator (*vide infra*) (Box 2C).

In biological systems, however, many of the molecules to be studied by vibrational spectroscopy lack any symmetry element, such that application of group theory to the analysis of vibrational spectra is restricted to only a few examples. Thus, this topic will not be covered comprehensively in this tutorial, but interested reader should consult specialised monographs (see Box 2B) (Wilson et al. 1955; Cotton 1990).

Essential support for the empirical vibrational analysis is based on isotopically labelled derivatives. A variation of the masses only alters the *G*-matrix and leaves the *F*-matrix unchanged. For the simplest case of a diatomic molecule, Eq. (2.11) shows that the frequency varies with the square root of the reciprocal reduced mass. However, for a three-atomic molecule the situation is even more complicated as the individual modes include contributions from three internal coordinates, albeit to different extents. Thus, force constants may be fitted to the experimental data set constituted by the vibrational frequencies of all isotopomers. Whereas for simple molecules with up to 10 atoms this approach has been applied with considerable success, it rapidly approaches practical limitations with an increasing number of atoms, because the synthetic efforts to produce a sufficiently large number of isotopically labelled compounds becomes enormous. Thus, the vibrational problem is inherently underdetermined.

Nevertheless, until the beginning of the 1990s, the empirical vibrational analysis was the only practicable way to extract structural information from the spectra of biological molecules such as porphyrins or retinals (Li et al. 1989, 1990a, 1990b; Curry et al. 1985). The starting point for this approach is a set of empirical force constants that have been found to be appropriate for specific internal coordinates. These force constants are derived from molecules for which a spectroscopic determination of the force field is facilitated due to the smaller size, higher

symmetry, and the availability of appropriate isotopomers. Subsequently, the force constant matrix of the molecule under consideration is simplified by appropriate approximations, including the neglect of interaction force constants for internal coordinates of widely separated parts of the molecule. Finally, the normal modes are calculated for the presumed geometry (*G*-matrix) and adjustments of individual force constants are made to achieve the best possible agreement with the experimental data. This refinement represents the most critical step as it requires a pre-assignment of the experimentally observed bands. Inconsistencies in the assignment and substantial deviations between calculated and experimental frequencies that can only be removed by choosing unusual force constants may then be taken as an indication that the presumed geometry was incorrect. The procedure is then repeated on the basis of alternative molecular structures until a satisfactory agreement between theory and experiment is achieved. It is fairly obvious that the reliability of such a tedious procedure strongly depends on the availability of a sufficiently large set of experimental data.

2.1.4
Quantum Chemical Calculations of the *FG*-Matrix

The alternative approach is to calculate the force constant matrix by quantum chemical methods, which, due to progress in the development of the hardware and efficient and user-friendly program packages, are nowadays applicable to biological molecules, including molecules of more than 50 non-hydrogen atoms. In these methods, an initial ("guess") geometry of a molecule is set up and the Schrödinger equation is solved in self-consistent field calculations, which lead to the energy eigenvalues for this geometry. Systematic variations of internal coordinates then eventually afford the geometry of lowest energy. This energy optimisation allows determination of the force constants by calculating the second derivatives of the potential energy according to Eq. (2.17). Thus, all elements of the *F*- and *G*-matrix can be computed and the normal modes are determined as described above.

The most promising quantum chemical method is based on density functional theory (DFT), which represents an excellent compromise between accuracy and computational costs. Unlike Hartree–Fock procedures, DFT is directed to calculated electron densities rather than wavefunctions. Within this approach, the energy depends on the electron density and this dependency is included in a functional. There are various functionals that have been suggested and tested for calculating different observables. For calculations of vibrational frequencies, the B3LYP functional is widely used and it was found to reproduce experimental data in a satisfactory manner when using a standard 6-31G* basis set (Rauhut and Pulay 1995). Nevertheless, the underlying approximations cause deviations from the experimental frequencies that are approximately in the order of 4%, corresponding to a frequency uncertainty of ca. ± 60 cm^{-1} for modes between 1500 and 1700 cm^{-1}. Considering a medium-sized molecule of 25 atoms, one may expect ca. 50 normal modes in the spectral region between 200 and 1700 cm^{-1} that
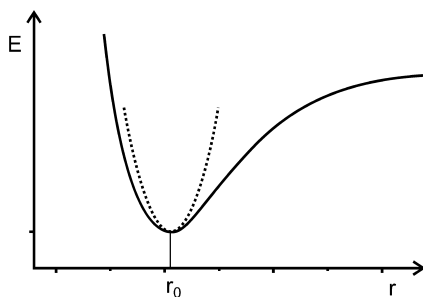
Fig. 2.4 Potential curves for a diatomic oscillator as a function of the inter-atomic distance *r*. The solid line is a schematic representation of a Morse potential function for an anharmonic oscillator whereas the dotted line refers to the harmonic potential function.

is usually studied by IR and Raman spectroscopy. This corresponds to an average density of modes of ca. 1 mode per 30 cm^{-1}, such that an accuracy of 4% for the calculated frequencies would not allow an unambiguous assignment for all experimentally observed bands.

The errors associated with the DFT calculations result from insufficient consideration of the electron correlation, and, more severely, from the harmonic approximation. The latter effect, illustrated in Fig. 2.4, causes an overestimation of the force constants, as the harmonic potential function is too narrow compared with an anharmonic potential function. These deficiencies of the DFT approach are systematic in nature such that they may be compensated *a posteriori*.

The simplest procedure is to correct the frequencies uniformly by multiplication with an empirical factor. This frequency scaling increases the accuracy of the calculated frequencies to ca. ± 25 cm^{-1}, which, however, is at the limit for an unambiguous vibrational assignment for molecules that include up to 50 atoms.

The most reliable procedure to correct for the intrinsic deficiencies of the quantum chemical calculations is to scale the force field directly. Using scaling factors σ_i that are specific for the various internal coordinates i, one obtains corrected force constants $(F_{ij})_\sigma$ according to

$$(F_{ij})_\sigma = \sqrt{\sigma_i}(F_{ij})\sqrt{\sigma_j} \tag{2.40}$$

These scaling factors can be determined for small example molecules for which a sound assignment of the experimental bands is established, such that the specific correction factors can be adjusted to yield the best agreement between calculated and experimental data (Rauhut and Pulay 1995; Magdó et al. 1999). The scaling factors are characteristic of specific internal coordinates but not unique for an individual molecule. Thus, they can be transferred to the target molecule and used without any further fine tuning. This concept of global scaling factors has been shown to provide an accuracy of ca. ± 10 cm^{-1} for the calculated frequencies,

even for large molecules. Attention has to be paid in the case of hydrogen bonded systems as here the 6-31G* basis set may not be sufficiently large (Mroginski et al. 2005). Applying the global scaling approach, however, requires a coordinate transformation of the force field from Cartesian to internal coordinates, which is not a routine procedure in each case (*vide supra*).

Even on the basis of scaled quantum chemical force fields, the comparison with the calculated frequencies alone does not allow for an unambiguous assignment for many biologically molecules as large as, for example, tetrapyrroles or retinals. Therefore, calculated band intensities are often required as additional assignment criteria. Calculation of IR and Raman intensities is straightforward within the software packages for quantum chemical methods used for the force field calculations. For resonance Raman intensity calculations, tailor-made solutions have to be designed (see Section 2.2.3).

2.2
Intensities of Vibrational Bands

Besides the frequencies of a normal mode, the intensity of the vibrational band is the second observable parameter in the vibrational spectrum. The intensity is simply proportional to the probability of the transition from a vibrational energy level n to the vibrational level m, typically (but not necessarily) corresponding to the vibrational ground and excited states, respectively. To understand the probabilities of transitions between different states that are induced by the interaction of the molecule with electromagnetic radiation, quantum mechanical treatments are required.

Generally, the transition probability P_{nm} is given by the square of the integral

$$P_{nm} = \langle \psi_m^* | \hat{\Omega} | \psi_n \rangle \tag{2.41}$$

where ψ_n and ψ_m are the wavefunctions for the vibrational states n and m, and $\hat{\Omega}$ is the operator that describes the perturbation of the molecule by the electromagnetic radiation. This operator is different for the physical processes in IR and Raman spectroscopy and is obtained by first-order and second-order perturbation theory, respectively.

2.2.1
Infrared Absorption

In IR spectroscopy, the transition $n \rightarrow m$ results from the absorption of a photon and thus the process is controlled by the electrical dipole moment operator $\hat{\mu}_q$, which is defined by

$$\hat{\mu}_q = \sum_\alpha e_\alpha \cdot q_\alpha \tag{2.42}$$

where e_α is the effective charge at the atom α and q_α is the distance to the centre of gravity of the molecule in Cartesian coordinates ($q = x, y, z$) (Wilson et al. 1955). The interaction with the radiation is given by the scalar product between the vector of the electric field of the radiation and $\hat{\mu}_q$. Averaging over all molecule orientations, the IR intensity for this transition is expressed by

$$I_{nm,\,\text{IR}} \propto ([\mu_x]_{nm}^2 + [\mu_y]_{nm}^2 + [\mu_z]_{nm}^2) \tag{2.43}$$

where $[\mu_q]_{nm}$ is the integral

$$[\mu_q]_{nm} = \langle \psi_m^* | \hat{\mu}_q | \psi_n \rangle \tag{2.44}$$

One can easily see that a vibrational transition $n \rightarrow m$ in the IR spectrum only occurs if it is associated with a non-zero transition dipole moment $[\mu_q]_{nm}$. To decide whether or not, a normal mode is IR active, we expand $\hat{\mu}_q$ in a Taylor series with respect to the normal coordinates Q_k. Within the harmonic approximation, the series is restricted to the linear terms

$$\hat{\mu}_q = \mu_q^0 + \sum_{K=1}^{3N-6} \hat{\mu}_q^k Q_k \tag{2.45}$$

with

$$\hat{\mu}_q^k = \left(\frac{\partial \mu_q}{\partial Q_k} \right)_0 \tag{2.46}$$

With Eq. (2.41) the transition probability is then given by

$$[\hat{\mu}_q] = \langle \psi_m^* | \hat{\mu}_q | \psi_n \rangle = \mu_q^0 \langle \psi_m^* \psi_n \rangle + \sum_{k=1}^{3N-6} \hat{\mu}_q^k \langle \psi_m^* | Q_k | \psi_n \rangle \tag{2.47}$$

The first integral on the right-hand side of Eq. (2.47) is zero as the wavefunctions ψ_n and ψ_m are orthogonal. Thus, a non-zero transition probability is only obtained if two conditions are fulfilled. Firstly, the derivative of the dipole moment with respect to the normal coordinate Q_k in Eq. (2.47) must be non-zero, which requires that the normal mode is associated with a change in the dipole moment. Secondly, the integral $\langle \psi_m^* | Q_k | \psi_n \rangle$ must be non-zero, which is the situation when the vibrational quantum numbers n and m differ by one. This implies that only fundamentals are IR active within the harmonic approximation.

Equation (2.47) holds for all three Cartesian coordinates such that only one non-zero transition dipole moment $[\mu_q]_{nm}$ ($q = x, y, z$) is sufficient to account for the IR intensity of the normal mode Q_k according to Eq. (2.43) (Box 2C). Using unpolarised light and randomly oriented molecules, the experiment does not allow the conclusion to be made as to which of the components of the transition
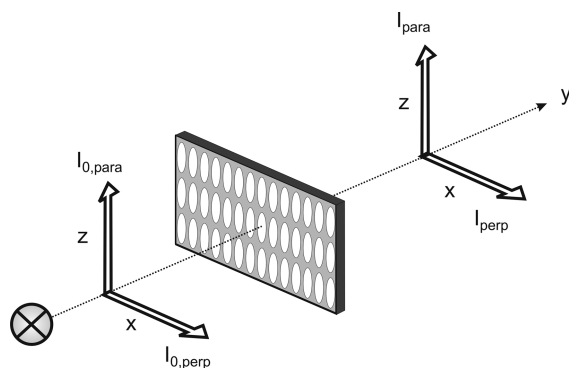
Fig. 2.5 IR dichroism of oriented molecules. The absorbance of light polarised parallel to the long molecular axis A_{para} is given by the ratio $I_{\mathrm{para}}/I_{0,\mathrm{para}}$ whereas the perpendicular component is defined by $I_{\mathrm{perp}}/I_{0,\mathrm{perp}}$.

dipole moment contributes to the IR intensity. If, however, the probe light is linearly polarised, it is possible to address the individual components of the transition dipole moments. Then IR measurements may provide additional information for the vibrational assignment, the orientation of the molecules with respect to the plane of polarisation of the incident light, or the orientation of a molecular building block within a macromolecule if the macromolecule itself is oriented.

Consider, for example, a sample of ellipsoidal molecules that are all oriented with the long axis in z-direction (Fig. 2.5). The incident light, propagating in the y-direction, can be polarised in z- or x-direction, corresponding to a parallel and perpendicular orientation of electric field vector, respectively. Parallel polarised light will thus specifically probe those vibrational modes that exhibit a transition dipole moment in the z-direction, and the absorbance A_{para} is given by

$$A_{\mathrm{para}} \propto |\mu_{mn}|_z^2 \tag{2.48}$$

If the molecules do not exhibit a preferential orientation in the xy plane, IR absorption of perpendicular polarised light depends on both the x- and the y-component of transition dipole moment

$$A_{\mathrm{perp}} \propto (|\mu_{mn}|_x^2 + |\mu_{mn}|_y^2) \tag{2.49}$$

The quantities A_{para} and A_{perp} are combined in the dichroic ratio d which is defined by

$$d = \frac{A_{\mathrm{para}} - A_{\mathrm{perp}}}{A_{\mathrm{para}} + A_{\mathrm{perp}}} \tag{2.50}$$

and which may vary between 1 and -1 for the limiting cases of $A_{\mathrm{perp}} = 0$ and $A_{\mathrm{para}} = 0$, respectively.
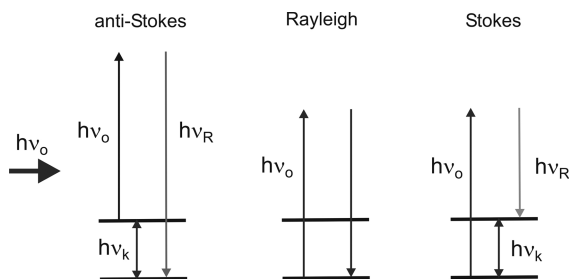
Fig. 2.6 Energy diagram representing the elastic Rayleigh scattering (centre) and the inelastic anti-Stokes (left) and Stokes (right) Raman scattering with v_0, v_R, and v_k referring to the frequencies of the incident light, the Raman scattered light, and the molecular vibration, respectively.

2.2.2
Raman Scattering

Raman spectroscopy differs principally from IR spectroscopy in that it is based on the scattering of photons by molecules rather than on the absorption of photons (Fig. 2.6). This scattering process can be illustrated readily on the basis of classical physics. Consider a molecule interacting with an electromagnetic wave with the electric field vector oscillating with the frequency v_0

$$\vec{E} = \vec{E}_0 \, \cos(2\pi v_0 t) \tag{2.51}$$

The oscillating electric field can induce a dipole in the molecule

$$\vec{\mu}_{ind} = \tilde{\alpha}(v) \cdot \vec{E}_0 \, \cos(2\pi v_0 t) \tag{2.52}$$

where $\tilde{\alpha}(v)$ is the polarisability. This quantity, which is actually a tensor, varies with time as it describes the response of the electron distribution to the movements of the nuclei that oscillate with the normal mode frequency v_k. Thus, we can express $\tilde{\alpha}(v)$ by

$$\tilde{\alpha}(v) = \tilde{\alpha}_0(v_0) + \left(\frac{\partial \tilde{\alpha}}{\partial Q_k}\right)_0 (2\pi v_k t) \tag{2.53}$$

Combining Eqs. (2.52 and 2.53) we obtain

$$\vec{\mu}_{ind} = \vec{E}_0 \left[\tilde{\alpha}_0(v_0) + \left(\frac{\partial \tilde{\alpha}}{\partial Q_k}\right)_0 \cos(2\pi v_k t) \right] \cos(2\pi v_0 t) \tag{2.54}$$

which eventually yields

$$\vec{\mu}_{ind} = \vec{E}_0 \left[\tilde{\alpha}_0 \cos(2\pi v_0 t) + \left(\frac{\partial \tilde{\alpha}}{\partial Q_k} \right)_0 Q_k \cos[2\pi(v_0 + v_k)t] \right.$$

$$\left. + \left(\frac{\partial \tilde{\alpha}}{\delta Q_k} \right)_0 Q_k \cos[2\pi(v_0 - v_k)t] \right] \tag{2.55}$$

The sum on the right side of Eq. (2.55) includes three terms corresponding to polarisabilities that depend on different frequencies, which are the frequency of the incident radiation v_0 and the frequencies $(v_0 - v_k)$ and $(v_0 + v_k)$ that differ from v_0 by the frequency of the normal mode. Scattering that leaves the frequency of the incident light unchanged is referred to as elastic or Rayleigh scattering whereas the frequency-shifted (inelastic) scattering is referred to as Raman scattering (Fig. 2.6). When the frequency of the scattered light is lower than v_0, the molecule remains in a higher vibrationally excited state ($m > n$ for the transition $n \rightarrow m$). This process is denoted as Stokes scattering whereas anti-Stokes scattering refers to $(v_0 + v_k)$ and thus to $m < n$. At ambient temperature, thermal energy is lower than the energies of most of the normal modes, such that molecules predominantly exists in the vibrational ground state and Stokes scattering represents the most important case of Raman scattering.

The energy conservation for Raman scattering is not contained in the classical treatment. It requires the quantum mechanical description of vibrational quantum states interacting with electromagnetic radiation (Placzek 1934). The operator, which according to Eq. (2.41) determines the probability of the Raman transition $n \rightarrow m$, is the polarisability $\hat{\alpha}$ with components defined by the molecule-fixed coordinates x, y, z.

$$\begin{bmatrix} \mu_{ind,x} \\ \mu_{ind,y} \\ \mu_{ind,z} \end{bmatrix} = \begin{bmatrix} \alpha_{xx} & \alpha_{xy} & \alpha_{xz} \\ \alpha_{yx} & \alpha_{yy} & \alpha_{yz} \\ \alpha_{zx} & \alpha_{zy} & \alpha_{zz} \end{bmatrix} \cdot \begin{bmatrix} E_x \\ E_y \\ E_z \end{bmatrix} \tag{2.56}$$

It is useful to define the Raman scattering cross section for the vibrational $n \rightarrow m$ transition $\sigma_{n \rightarrow m}$ by

$$I_{n \rightarrow m} = \sigma_{n \rightarrow m} I_0 \tag{2.57}$$

where I_0 is the intensity of the incident radiation and $I_{n \rightarrow m}$ is the scattered intensity integrated over all scattering angles and polarisation directions for a non-oriented sample. The Raman cross section is correlated with the Raman polarisability by

$$\sigma_{n \rightarrow m} \propto (v_0 \pm v_k)^4 \cdot \sum_{\rho, \sigma} |\alpha_{\rho, \sigma}|^2 \tag{2.58}$$

taking into account that the intensity for electric dipole radiation scales with the fourth power of the frequency. The indices ρ and σ denote the molecule-fixed coordinates.
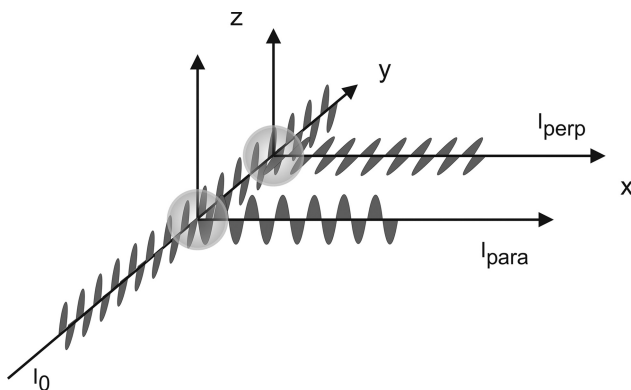
Fig. 2.7 Illustration of polarised Raman scattering in a 90°-scattering geometry. I_{perp} and I_{para} are the respective perpendicular and parallel components of the Raman scattering with respect to the polarisation of the incident monochromatic radiation.

The tensor properties of $\alpha_{\rho\sigma}$ have consequences for the polarisation of the Raman scattered light. This can easily be illustrated for molecules that are oriented with respect to the electric field vector of the incident excitation radiation, which is usually highly polarised laser light (Fig. 2.7). If we now refer the molecule-fixed coordinate system to the directions of the electric field vector (z-axis), of the propagation of the laser light (y-axis), and of the detection of the scattered light (x-axis), the intensity of the Raman scattered radiation includes two components, which are polarised parallel (I_{para}) and perpendicular (I_{perp}) with respect to the electric field vector of the incident light, and only depend on the tensor components α_{zz} and α_{yz}, respectively.

$$I_{\text{para}} \propto |\alpha_{zz}|^2 \cdot |\vec{E}_z|^2$$
$$I_{\text{perp}} \propto |\alpha_{yz}|^2 \cdot |\vec{E}_z|^2 \tag{2.59}$$

Appropriate re-alignment of the oriented sample with respect to the laser beam then allows the remaining tensor components to also be determined, taking into account that the scattering tensor is symmetric, i.e., $\alpha_{\sigma\rho} = \alpha_{\rho\sigma}$.

In the general case of non-oriented molecules, the relationship between the polarisation properties of the Raman scattered light and the scattering tensor is more complicated and the individual tensor components cannot be determined directly. For the depolarisation ratio ρ, which is defined by the ratio of perpendicular polarised and parallel polarised Raman scattered light, one obtains

$$\rho = \frac{I_{\text{perp}}}{I_{\text{para}}} = \frac{3\gamma_{\text{s}}^2 + 5\gamma_{\text{as}}^2}{45\bar{\alpha}^2 + 4\gamma_{\text{s}}^2} \tag{2.60}$$

with the mean polarisability $\bar{\alpha}$ and the symmetric (γ_s) and antisymmetric (γ_{as}) anisotropy given by

$$\bar{\alpha} = \frac{1}{3}\sum_{\rho\rho}\alpha_{\rho\rho}$$

$$\gamma_s^2 = \frac{1}{2}\sum_{\rho\sigma}(\alpha_{\rho\rho} - \alpha_{\sigma\sigma})^2 + \frac{3}{4}\sum_{\rho\sigma}(\alpha_{\rho\sigma} + \alpha_{\sigma\rho})^2 \qquad (2.61)$$

$$\gamma_{as}^2 = \frac{3}{4}\sum_{\rho\sigma}(\alpha_{\rho\sigma} - \alpha_{\sigma\rho})^2$$

In the case of symmetric molecules, determination of polarisation ratios is a useful tool for the vibrational assignment. For each symmetry species of a point group, the character table indicates which of the individual tensor components are zero and which are non-zero (Wilson et al. 1955; Czernuszewicz and Spiro 1999) (Box 2C). On this basis, it is not only possible to decide if the modes of this species are Raman-active, but also to predict the polarisation ratio, which can then be compared with the experimentally observed value.

As in IR absorption spectroscopy, a description of Raman intensities is only possible on the basis of a quantum mechanical treatment (Placzek 1934). In Raman scattering two photons are involved, hence second-order perturbation theory is required. On the basis of Kramers–Heisenberg–Dirac's dispersion theory, the scattering tensor is expressed as

$$[\alpha_{nm}]_{\rho\sigma} = \frac{1}{h}\sum_{R,r}\left(\frac{\langle nG|M_\rho|Rr\rangle\langle rR|M_\sigma|Gm\rangle}{v_{Rr} - v_k - v_0 + i\Gamma_R} + \frac{\langle rR|M_\sigma|Gm\rangle\langle nG|M_\rho|Rr\rangle}{v_{Rr} - v_k + v_0 + i\Gamma_R}\right) \qquad (2.62)$$

where $M_\sigma(M_\rho)$ is the electronic transition dipole moment in terms of a molecule-fixed coordinate system (Albrecht 1961; Warshel and Dauber 1977). The symbols v_0 and v_k denote the frequency of the excitation radiation and the normal mode Q_k, respectively (Fig. 2.6). The indices "R" and "r" refer to the respective electronic and vibrational (vibronic) states of the molecule and Γ_R is a damping constant that is related to the lifetime of the vibronic state Rr. Equation (2.62) represents a sum of integrals that describe the transitions $nG \to Rr$ and $Rr \to Gm$. The sum indicates that for the Raman transition all vibronic states have to be considered. This implies that the scattering tensor and thus the Raman intensity is controlled by the transition probabilities involving all vibronic states, even though the initial and final states refer to the vibrational ground and excited states of the electronic ground state.

In the general case, the energy of the exciting radiation hv_0 is much lower than the energy of any vibronic transition hv_{Rr}. Let us consider an example of a molecule with the first four electronic transitions E_i at 300, 240, 200, and 180 nm. Using an excitation line at 1064 nm and neglecting the damping terms, we can determine the relative weights of the individual terms in the sum of Eq. (2.62),
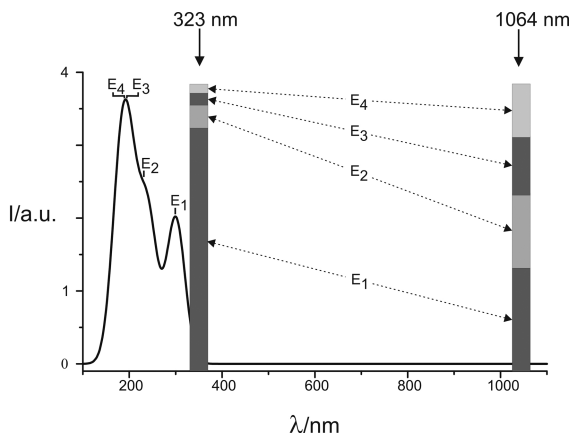
Fig. 2.8 Absorption spectrum of a molecule with four electronic transitions (E_1, E_2, E_3, and E_4). The columns represent the frequency-dependent weights of the electronic transitions to the scattering tensor [Eq. (2.62)] for excitation lines at 1064 and 323 nm. The calculations refer to a vibrational mode at 1500 cm^{-1}.

as given by the denominators, i.e., $(v_{Rr} - v_0 - v_k)^{-1}$ and $(v_{Rr} + v_0 - v_k)^{-1}$ (Fig. 2.8). One can easily see that under these conditions the contributions of the four electronic states to the scattering tensor are comparable, as shown for the normal mode v_k at 1500 cm^{-1}. The situation is different when the excitation energy approaches the energy of an electronic transition. Then, for this specific transition the term $(v_{Rr} - v_0 - v_k)^{-1}$ dominates over all other terms in the sum of Eq. (2.62). This is demonstrated for $v_0 = 30\,960$ cm^{-1} (323 nm) for which the contribution from the first electronic transition is more than 10 times larger than that from the second transition.

2.2.3
Resonance Raman Effect

The conditions under which v_0 is close to the frequency of an electronic transition refer to the resonance Raman (RR) effect, for which Eq. (2.62) consequently can be simplified to

$$[\alpha_{nm}]_{\rho\sigma} \cong \frac{1}{h} \sum_r \left(\frac{\langle nG|M_\rho|Rr\rangle\langle rR|M_\sigma|Gm\rangle}{v_{Rr} - v_k - v_0 + i\Gamma_R} \right) \tag{2.63}$$

where summation is now restricted to the vibrational states r of the resonant electronically excited state (Albrecht 1961; Warshel and Dauber, 1977). In contrast to Eq. (2.44), the wavefunctions of the integrals in Eq. (2.63) depend on the elec-

tronic and nuclear coordinates, which can be separated within the Born–Oppenheimer approximation according to

$$\langle nG|M_\rho|Rr\rangle = \langle nr\rangle\langle G|M_\rho|R\rangle = \langle nr\rangle M_{GR,\rho} \tag{2.64}$$

Here, integrals of the type $\langle nr\rangle$ represent the Franck–Condon factors that are the integrals over the products of two vibrational wavefunctions. With this approximation, Eq. (2.63) leads to

$$[\alpha_{nm}]_{\rho\sigma} \cong \frac{1}{h}\sum_r\left(\frac{\langle nr\rangle\langle rm\rangle M_{GR,\rho}M_{GR,\sigma}}{v_{Rr} - v_k - v_0 + i\Gamma_R}\right) \tag{2.65}$$

The electronic transition dipole moment components $M_{GR,\rho}$ which refer to the electronic transition from the ground state G to the (resonant) electronically excited state R, can now be expanded in a Taylor series with respect to the normal coordinates Q_k.

$$M_{GR,\rho}(Q_k) = M_{GR,\rho}(Q_k^{(0)}) + \sum_k\left(\frac{\partial M_{GR,\rho}}{\partial Q_k}\right)_0 Q_k + \cdots\cdots \tag{2.66}$$

Within the harmonic approximation we neglect higher order terms and combine Eqs. (2.65 and 2.66) to obtain the scattering tensor as the sum of two terms, the so-called Albrecht's *A*- and *B*-terms.

$$[\alpha_{nm}]_{\rho\sigma} \cong A_{\rho\sigma} + B_{\rho\sigma} \tag{2.67}$$

with

$$A_{\rho\sigma} \cong \frac{1}{h}\sum_r\left(\frac{\langle nr\rangle\langle rm\rangle M_{GR,\rho}^0 M_{GR,\sigma}^0}{v_{Rr} - v_k - v_0 + i\Gamma_R}\right) \tag{2.68}$$

where $M_{GR,\rho}^0$ and $M_{GR,\sigma}^0$ are the components of transition dipole moment of the vertical electronic transition $G \rightarrow R$. The *B*-term is given by

$$B_{\rho\sigma} \cong \frac{1}{h}\sum_r\left(\frac{\langle n|Q_k|r\rangle\langle rm\rangle\left(\frac{\partial M_{GR,\rho}}{\partial Q_k}\right)_0 M_{GR,\sigma}^0}{v_{Rr} - v_k - v_0 + i\Gamma_R} + \frac{\langle nr\rangle\langle r|Q_k|m\rangle\left(\frac{\partial M_{GR,\sigma}}{\partial Q_k}\right)_0 M_{GR,\rho}^0}{v_{Rr} - v_k - v_0 + i\Gamma_R}\right) \tag{2.69}$$

The *A*- and *B*-terms represent different scattering mechanisms; however, common to both terms is that the dominators rapidly decrease when the frequency of the excitation line v_0 approaches the frequency of an electronic transition. Then both the *A*- and the *B*-terms and thus the RR intensity increase [Eqs. (2.57

and 2.58)], albeit to a different extent depending on the character of the electronic transitions and normal modes involved.

When the resonant electronic transition exhibits a large oscillator strength, that is a large transition dipole moment M_{GR}^0, the *A*-term, which scales with $|M_{GR}^0|^2$, increases more significantly than the *B*-term and thus becomes the leading term. Then the enhancement of a normal mode depends on the Franck–Condon factor products $\langle nr \rangle \langle rm \rangle$ (Franck–Condon enhancement). Whether or not, a normal mode is resonance enhanced via the Franck–Condon mechanism, depends on the geometry of the resonant excited state.

Consider, for example, ethylene, which exhibits a strong electronic absorption band at ca. 200 nm, originating from the (first) allowed $\pi \to \pi^*$ transition of the C=C double bond. Population of the π^* orbital leads to the lowering of the bond order from 2 to 1, implying that in this excited state the C–C bond length increases. Hence, the potential energy curve for the C–C distance is displaced in this electronically excited state with respect to the ground state, as shown in Fig. 2.9, i.e., along the main internal coordinate of this normal mode. Now we must consider the Franck–Condon factors that couple the wavefunctions of the ground and excited state. According to Eq. (2.68), we have to sum up over those integrals that involve all vibrational states of the electronic excited state, with their relative weight being determined by the match with the excitation energy. For the sake of simplicity we will restrict the discussion to the RR transition $n \to m$ exclusively
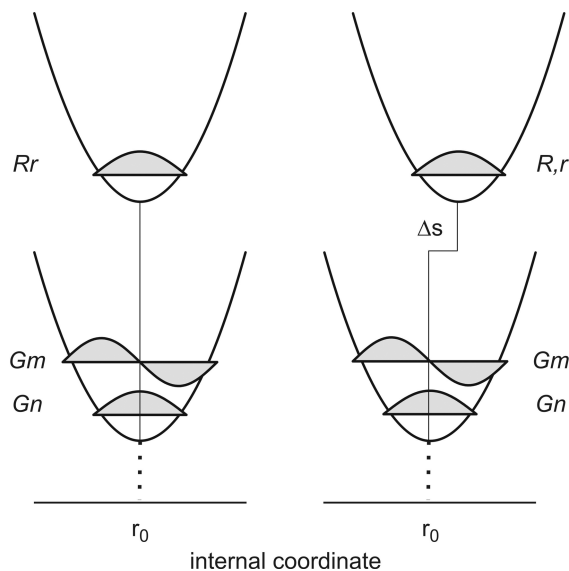

Fig. 2.9 Harmonic potential curves for the electronic ground (*G*) and excited state (*R*), illustrating the situation for an excited state displacement of $\Delta s = 0$ (left) and $\Delta s \neq 0$ (right) for RR transitions from the vibrational ground state *Gn* to the first vibrationally excited state *Gm* via coupling to the vibronic state *Rr*.

via the vibronic state Rr such that we only consider one term of the sum, i.e., the integrals involving the vibronic state Rr (Fig. 2.9). The wavefunctions of the first integral $\langle nr \rangle$ have the same symmetry, but due to the potential curve displacement in the direction of the internal coordinate of this mode the integral is non-zero, albeit smaller than one. For the same reason, the wavefunctions of the integral $\langle rm \rangle$ that have different symmetries are not zero either. Similar considerations hold for Franck–Condon factors involving other vibronic states. This implies that a vibrational mode including the C=C stretching coordinate exhibits non-zero Franck–Condon factor products and thus gains resonance Raman (RR) intensity via the *A*-term scattering mechanism (Box 2C).

The situation is different for modes including the C–H stretching coordinate (Fig. 2.9). As the C–H distance remains unaffected upon the $\pi \to \pi^*$ electronic transition, the origin of the corresponding potential curve is at the same position in the electronic ground and excited states. In this instance the integral $\langle nr \rangle$ will be non-zero but the $\langle rm \rangle$ integral will vanish, implying that a pure C–H stretching mode will not be RR active. The fact that C–H stretching modes are Raman-active instead just reflects the involvement of higher lying electronic transitions, amongst which at least one is associated with a geometry change of the C–H stretching coordinate.

The importance of excited-state displacements for the RR intensity can be generalised (Warshel and Dauber 1977). Only modes including at least one internal coordinate that changes with the electronic transition can gain resonance enhancment via the *A*-term mechanism. The relationship between the excited state displacement Δs and the *A*-term contribution to the scattering tensor can be approximated by

$$A \propto \frac{|M^0_{GR}|^2 \cdot v_k \cdot \Delta s}{(v_{Rr} - v_0 + i\Gamma_R)(v_{Rr} - v_0 + v_k + i\Gamma_R)} \tag{2.70}$$

This expression assumes that the normal modes do not change in the electronic excited state, both with respect to their composition and with respect to the frequency. Although this appears to be a severe restriction, Eq. (2.70) has been shown to provide a good basis for qualitative predictions of the RR activity of modes that are dominated by one internal coordinate, given that the nature of the resonant excited state is known. The situation is much more complicated for modes involving many internal coordinates to comparable extents, and *a priori* predictions are impossible. The contributions from different internal coordinates to Δs may have positive or negative sign, such that they can be additive or cancel each other (Mroginski et al. 2003).

Calculation of RR intensities still represents a challenge as both ground state (structure, vibrational frequencies) and excited state properties (excitation energies, structure) have to be treated. In a particularly promising concept, quantum mechanical calculations are combined with the use of experimental data. Within the framework of the so-called Transform theory, the frequency dependence of the *A*-term of the scattering tensor [Eq. (2.70)] may be obtained by the Kramers–

Kronig transformation of the absorption band (Peticolas and Rush 1995). The electronic transition dipole moments M_{GR}^0 and the excited state displacements of a given normal mode Δs are calculated by quantum chemical methods such as time-dependent DFT. At present, these approaches are still fairly time-consuming and, specifically, the calculation of excited state geometries, required for determining Δs, is not trivial, even for relatively small molecules.

The crucial parameter that controls resonance enhancement via the *B*-term scattering mechanism is the derivative of the electronic transition dipole moment with respect to the normal mode (Albrecht 1961). This derivative is large for those modes that can effectively couple to an electronic transition and thus may gain RR intensity even when the resonant electronic transition is relatively weak. This vibronic coupling enhancement may also be operative when the excitation frequency is close to the frequencies of two electronic transitions.

An alternative approach to describe the Franck–Condon-type resonance enhancement (*A*-term scattering) has been developed by Heller who described the scattering process in terms of wave-packet dynamics (Heller 1981). As the temporal evolution of the scattering process is much faster than the nuclear vibrations, consideration of the summation over the multitude of vibronic eigenstates is definitely not necessary. The RR intensity is induced by the force $\partial V/\partial Q_k$ exerted by the excited state potential surface on the nuclear ground state configuration. This force controls the temporal evolution of the ground state wavefunction $|n(t)\rangle$ after excitation to the excited state surface and before returning to the final state $|m\rangle$. The RR intensity for a given mode k is then given by

$$I_{RR}(k) \propto \left[\int_0^{\infty} |M_{GR}^2 \cdot \exp(iv_0 t - \Gamma_r t) \cdot \langle m|n(t)\rangle \mathrm{d}t| \right]^2 \tag{2.71}$$

This expression is analogous to the square of Eq. (2.68). Furthermore, the treatments of the RR scattering in the time-domain by Heller (Heller 1981) and in the frequency domain via the Kramers–Heisenberg–Dirac dispersion relation are linked to each other through the Fourier transform. Also, in the time-domain treatment further simplifications can be introduced using similar assumptions as those used for Eq. (2.70). The advantage of Heller's approach is particularly evident for those instances where only a few internal coordinates exhibit large excited state displacements Δs and thus the RR spectrum is dominated only by a couple of normal modes. For these modes the RR intensities does not only depend on Δs but also on the magnitude of $\partial V/\partial Q_k$. The intensity ratio of two normal modes k and l is then given by

$$\frac{I_{RR}(k)}{I_{RR}(l)} = \frac{v_l}{v_k} \cdot \left(\frac{\partial V/\partial Q_k}{\partial V/\partial Q_l} \right)^2 \approx \frac{v_k^3 \cdot \Delta_k^2}{v_l^3 \cdot \Delta_l^2} \tag{2.72}$$

This approach has been successfully employed to analyse the RR spectra of metalloproteins upon excitation in resonance with charge-transfer transitions (Blair et al. 1985).

The expressions in Eqs. (2.67–2.72) represent approximations that can be employed when the contributions from one or two electronic transitions to the scattering tensor become dominant. Consequently, there is no sharp borderline between non-resonance Raman and RR scattering. Resonance enhancement simply means that the vibrational modes of a chromophore within a molecule selectively gain intensity when the excitation line is in resonance with an electronic transition. Such an enhancement does not necessarily require an exact frequency match of the excitation and the electronic transition. Indeed, a closer inspection of the frequency dependence of the Raman intensity reveals that a specific enhancement of these modes already occurs for excitation lines relatively far away from the maximum of the electronic transition. This is illustrated by comparing the frequency dependence of the Raman intensity under strictly non-resonance conditions [Eqs. (2.57 and 2.58)] and the RR intensity provided by the A-term scattering mechanism. In the latter, an approximate formula can be derived for the Stokes scattering under pre-resonance conditions (Albrecht and Hutley 1971), i.e., when the damping constant [Eq. (2.68)] can be neglected ($|v_R - v_0| \gg |\Gamma_R|$),

$$I_{nm, RR} \propto (v_0 - v_k)^4 \frac{(v_0 - v_k)^2 (v_0^2 + v_R^2)}{(v_R^2 - v_0^2)^2} \tag{2.73}$$

To compare the RR and Raman intensities, Eq. (2.73) has to be corrected for the "normal" v^4-dependence of the radiation intensity [Eqs. (2.57 and 2.58)]

$$\frac{I_{nm, RR}}{I_{nm, Ra}} \propto \frac{(v_0 - v_k)^2 (v_0^2 + v_R^2)}{(v_R^2 - v_0^2)^2} \tag{2.74}$$

The ratio $I_{nm, RR}/I_{nm, Ra}$ represents the resonance enhancement, which in Fig. 2.10 is plotted as a function of the frequency difference between the excitation and the the electronic transition. It can be seen that the enhancement factor solely associated with the frequency dependence of the scattering tensor strongly increases for $v_0 \rightarrow v_R$ and even for an energy gap of 5000 cm^{-1} it is nearly 500. For more rigorous resonance conditions, for which Eq. (2.74) is no longer valid, the resonance enhancement can reach 5–6 orders of magnitude, depending on the other quantities that control the scattering tensor, i.e., the Franck–Condon factor products, the square of the electronic transition dipole moment, and the damping constant [Eq. (2.68)]. As a rule of thumb, the resonance enhancement then scales with the square of the extinction coefficient of the electronic absorption band at the excitation line. Consequently, the sensitivity of Raman spectroscopy increases greatly under resonance conditions and approaches that of UV–vis absorption spectroscopy.

It should be emphasised at this point that the frequencies refer to the molecular structure in the initial electronic state, usually the electronic ground state, although the RR intensities are sensitively controlled by the properties of the electronically excited state(s). Resonance enhancement represents the gain in Raman
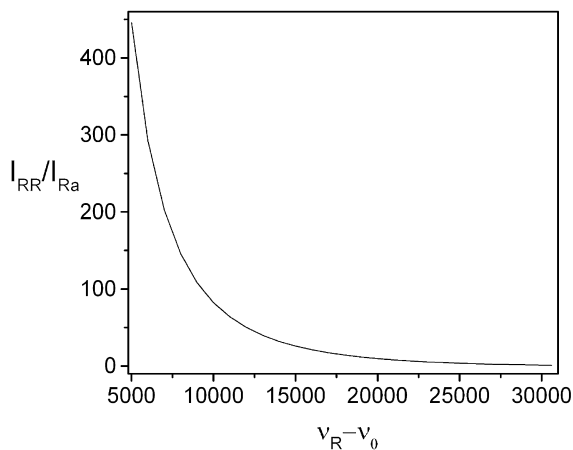
Fig. 2.10 Resonance enhancement I_{RR}/I_{Ra} via the *A*-term mechanism [Eq. (2.74)] as a function of the difference between the frequency of the incident light ν_0 and the electronic transition ν_R.

intensity for the vibrational bands of a chromophore as compared with strictly non-resonance conditions. It is restricted to that part of the molecule in which the resonant electronic transition is localised. Such a selective enhancement has enormous practical implications when we are interested in studying the vibrational spectrum of the specific constituents of a macromolecule, such as a cofactor within a protein. Choosing appropriate excitation lines will then allow probing the vibrational bands solely of the cofactor such that the non-resonant Raman bands of the apo-protein can be effectively discriminated in most instances.

2.3
Surface Enhanced Vibrational Spectroscopy

Thirty years ago it was discovered accidentally that molecules adsorbed on rough surfaces of certain metals may experience a drastic enhancement of the Raman scattering. This unexpected finding immediately prompted intensive research activities in this field. Initially, these studies were directed at elucidating the nature of this enormous enhancement, which could be of several orders of magnitude. Later, it was also recognised that this technique had a high potential for studying molecules at interfaces. Since that time, the surface enhanced Raman scattering (SERS) effect has become largely understood and this technique has found a place not only in surface and interfacial science but also in biophysics. Moreover, it was also noticed that the enhancement of vibrational bands at metal surfaces is not restricted to Raman scattering but may also take place, albeit to a smaller extent, in IR absorption, i.e., surface enhanced infrared absorption (SEIRA). SERS and SEIRA have been observed at metal interfaces with solid, liquid, or

gas (vacuum) phases, but only the solid/solution interface is of relevance in biological applications. The enhancement is metal- and wavelength-specific, such that for the typical spectral range of Raman and IR spectroscopy from 400 to 10000 nm, the metals that can be employed are Ag and Au.

2.3.1
Surface Enhanced Raman Effect

The SER effect can largely be understood on the basis of classical electromagnetic theory (Kerker et al. 1980; Moskovits 1985). The starting point is the analysis of light scattering and absorption by colloidal particles, which was considered about a century ago by G. Mie (Mie 1908). In a first approximation, colloidal particles can be represented as spheres. When the size of the particles is small with respect to the wavelength of the incident light (Rayleigh limit), the electromagnetic field can effectively couple with the collective vibrations of the ''free electrons'' of the metal, which are denoted as surface plasmons (Kerker et al. 1980; Moskovits 1985). The incident electric field $\vec{E}_0(v_0)$, oscillating with the frequency v_0, induces an electric dipole moment in the sphere and excites the surface plasmons, causing an additional electric field component $\vec{E}_{\text{ind}}(v_0)$, normal to the surface in the near-field of the sphere. Thus, the total electric field of the frequency v_0 is then expressed by

$$\vec{E}_{\text{tot}}(v_0) = \vec{E}_0(v_0) + \vec{E}_{\text{ind}}(v_0) \tag{2.75}$$

Since $\vec{E}_{\text{ind}}(v_0)$ is a function of $\vec{E}_0(v_0)$ the enhancement of the electric field is given by

$$F_E(v_0) = \frac{|\vec{E}_0(v_0) + \vec{E}_{\text{ind}}(v_0)|}{|\vec{E}_0(v_0)|} = |1 + 2g_0| \tag{2.76}$$

The quantity g_0 is related to the dielectric properties of the metal through

$$g_0 = \frac{\tilde{\varepsilon}_r(v_0) - 1}{\tilde{\varepsilon}_r(v_0) + 2} \tag{2.77}$$

Here $\tilde{\varepsilon}_r(v_0)$ is the frequency-dependent dielectric constant divided by the square of the refractive index of the surrounding medium n_{solv}.

$$\tilde{\varepsilon}_r(v_0) = \frac{\varepsilon_{re}(v_0) + i\varepsilon_{im}(v_0)}{n_{\text{solv}}^2} \tag{2.78}$$

Equations (2.76–2.78) show that g_0, and thus the field enhancement $F_E(v_0)$, becomes large if the real part of the relative dielectric constant approaches -2 and the imaginary part is small. These conditions depend on the wavelength and are,

within the Rayleigh limit, particularly well matched for Ag and Au colloids at ca. 400 and 560 nm, respectively.

A molecule that is located in close proximity to the sphere is excited by the electric field $\vec{E}_{tot}(v_0)$, which may induce all possible photophysical and photochemical processes, including Raman scattering. If the resonance conditions are fulfilled for the incident light with v_0, this will also be approximately the case for the frequency of the Raman scattered light $v_0 \pm v_k$. Then, the electric field of the Raman scattered light, $\vec{E}_{Ra}(v_0 \pm v_k)$, of the normal mode k that is proportional to $\vec{E}_{tot}(v_0)$ also induces a secondary electric field component $\vec{E}_{Ra,ind}(v_0 \pm v_k)$ in the metal particle giving rise to a total electric field oscillating with $v_0 \pm v_k$ in analogy to Eq. (2.75). Thus, Eq. (2.76) holds for both the electric field of the exciting and the Raman scattered light. As the intensity of the Raman scattered light in the far field is proportional to $|\vec{E}_{Ra,tot}(v_0 \pm v_k)|^2$, the total surface enhancement factor of the Raman intensity is given by

$$F_{SER}(v_0 \pm v_k) = [(1 + 2g_0)(1 + 2g_{Ra})]^2 \tag{2.79}$$

Equation (2.79) indicates that even a field enhancement by a factor of 10 yields an enhancement of the Raman intensity of more than 10^4.

These simple considerations hold for particles much smaller than the wavelength and are thus independent of the shape and the size of the particles. The enhancement at larger particles, however, is no longer shape- and size-independent. One can show that, in general, larger spheres or ellipsoidal shapes cause a red-shift of the wavelength of maximum enhancement. This is also true for interacting particles, i.e., aggregated colloids.

A particularly large enhancement is predicted for tips of the type used in scanning probe microscopy. These predictions have indeed been confirmed and utilised in so-called tip-enhanced Raman spectroscopy (Kneipp et al. 2006). In this technique, a sharp tip, as used for scanning tunnelling or atomic force microscopy, is brought into close proximity with that part of a molecular sample that is in the focus of the incident laser beam. Only the molecules in the near-field of the tip experience an enhancement of the Raman scattering.

For biological applications, metal electrodes represent more versatile SER-active devices as they allow probing of potential-dependent processes by controlling the electrode potential (Murgida and Hildebrandt 2004, 2005). The enhancement mechanism on electrodes can be largely understood within the same theoretical framework as outlined above for the SER effect on metal colloids. A submicroscopic roughness of the electrode, typically generated by electrochemical roughening (oxidation–reduction cycles), is a prerequisite for the SER effect on metal electrodes. The scale of this roughness is comparable to the dimensions of SER-active metal colloids, such that an SER-active electrode can be approximated by an array of metal semispheres, for which a treatment of the field enhancement similar to isolated metal spheres is possible. Taking into account that the scale of roughness which is produced by electrochemical roughening of the electrode surface is approximately the same as the dimension of SER-active colloids, one may
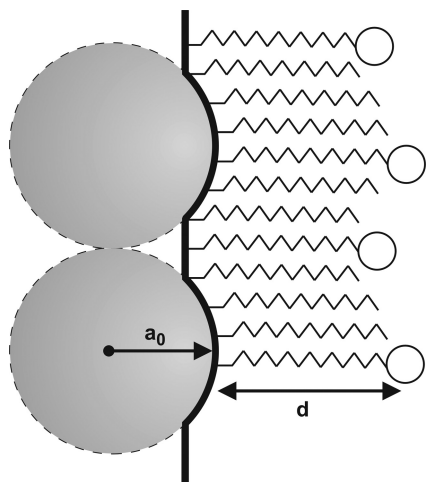
Fig. 2.11 Simplified view of a sub-microscopically rough metal surface (thick solid line) approximating the surface roughness for semi-spheres of radius a_0. Molecules contributing to the SER scattering (hollow spheres) are separated from the surface via spacers of length d.

approximate the roughness on electrodes by semi-spherical particles, or more appropriately, by connected semi-spheres (Fig. 2.11). In SER experiments, the surface roughness of electrodes is not uniform, corresponding to approximate semi-sphere structures with a wide distribution of particle radii a_0 (Fig. 2.12). Thus, the experimentally observed wavelength-dependent surface enhancement is very broad and may cover the entire spectral region from the resonance frequency at the Rayleigh limit ($a_0 \ll \lambda_0$) up to the infrared spectral region.
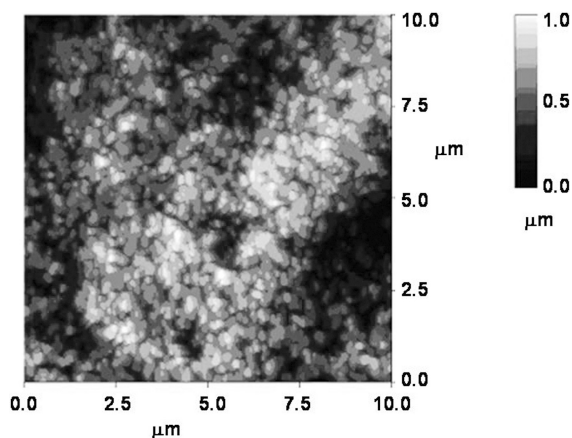

Fig. 2.12 Atomic force microscopic picture of an electrochemically roughened silver electrode.

In the relatively few instances for which the enhancement factor has been determined on the basis of the number of scattering molecules, values of 10^5–10^6 have been reported, which can be understood within the framework of the electromagnetic theory. Enhancement factors of this magnitude drastically increase the sensitivity of the Raman effect, such that SER spectroscopy represents a sensitive tool for studying molecules in the adsorbed state. The sensitivity, and, moreover, the selectivity can be further increased for molecules that exhibit an electronic absorption in the visible region. Then it is possible to tune the excitation frequency to be in resonance with both the electronic transition of the adsorbate and the surface plasmons of the metal. Under these conditions, the molecular RR and the SER effect combine (surface enhanced resonance Raman scattering – SERRS), such that it is readily possible to measure high quality spectra of molecules even if they are adsorbed at sub-monomolecular coverage. In fact, it has been shown that the effective quantum yield for the SERR process may approach unity (Hildebrandt and Stockburger 1984) and thus offers the possibility to probe even single molecules (Kneipp et al. 2006). If the chromophore associated with the resonant electronic transition is a cofactor in a protein, SERR spectroscopy displays a two-fold selectivity, as it probes selectively the vibrational spectrum of the cofactor of only the adsorbed molecules.

The electromagnetic theory of the SER effect implies that the enhancement is not restricted to molecules attached directly to the metal, although it decays according to the distance-dependence of dipole–dipole interactions. For spherical colloids of radius a_0 the decrease in the enhancement factor F_{SER} with the distance d from the surface is given by

$$F_{SER}(d) = F_{SER}(0) \cdot \left(\frac{a_0}{a_0 + d} \right)^{12} \tag{2.80}$$

where $F_{SER}(0)$ is the enhancement factor for molecules directly adsorbed onto the metal surface. For a particle radius of 20 nm, the enhancement is then estimated to decrease by a factor of ca. 10 when the molecule is separated by ca. 3.5 nm from the surface (Fig. 2.13). This prediction is in agreement with experimental findings and has also been verified for molecules immobilised on metal films and electrodes. Moreover, the consequences of this distance-dependence are important when applying SER spectroscopy to biological molecules. As direct interactions with the metal, specifically with Ag, may cause denaturation of biomolecules, it is advisable to cover the metal surfaces with biocompatible coatings that provide less harmful immobilisation conditions (see Section 4.3.6). The thickness of the coatings is typically between 1 and 5 nm, hence the surface enhancement is still sufficiently strong for the SER effect to be utilised (Murgida and Hildebrandt 2004, 2005).

In general, the electromagnetic theory provides a satisfactory explanation for the SER effect. However, there are a few documented cases that point to an additional contribution, which is commonly denoted as the "chemical effect" (Otto
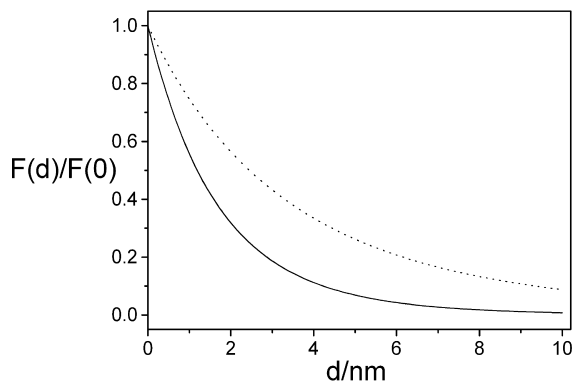
Fig. 2.13 Distance dependence of the surface enhancement for Raman
scattering [solid line – Eq. (2.80)] and IR absorption [dotted line –
Eq. (2.81)]. The surface roughness as defined in Fig. 2.11 is assumed
to be $a_0 = 20$ nm in each instance.

2001). This effect is restricted to molecules chemisorbed on sites of atomic-scale
roughness, such as ad-atoms on a surface. Such surface complexes represent es-
sentially new compounds in which electronic transitions associated with the elec-
tronic states of the metal atom are involved. These transitions are analogous to
charge transfer transitions of transition metal complexes. Excitation in resonance
with such a transition leads to the enhancement of the Raman bands of the ad-
atom–molecule complex similar to the molecular RR mechanism. This chemical
effect has been demonstrated for small molecules under conditions where
atomic-scale roughness is preserved, such as on cold-deposited metal films in an
ultrahigh vacuum at low temperature. It may also play a role in so-called "hot
spots" generated with metal nanoparticles and assumed to be crucial for single-
molecule SER spectroscopy (Kneipp et al. 2006). The chemical effect can be ne-
glected for those devices in which the probe molecules are not in direct contact
with the metal surface, such as in SERR spectroscopy of protein-bound cofactors
or for devices including biocompatible coatings. For this reason and due to the
low magnitude of the enhancement (ca. 100), the importance of the chemical ef-
fect in SER (SERR) spectroscopy of biological systems is small.

2.3.2
Surface Enhanced Infrared Absorption

The electromagnetic theory also provides the conceptual framework for under-
standing enhanced absorption of radiation by molecules adsorbed on or in close
vicinity to Ag or Au surfaces. In this instance, the optically active metal surfaces
are created by electrodeless deposition of Ag or Au in the vacuum or in solution
(Osawa 1997). The thin metal films that are usually deposited on an optically in-

ert support display a morphology of interconnected islands corresponding to a roughness similar to that created on massive electrodes by electrochemical procedures. The incident broad-band radiation induces an oscillating dipole in the metal islands which, in analogy to Eq. (2.76), leads to an increase in the electric field in the near-field, and thus to an enhanced absorption by molecules that are located in close proximity to the film. As only the electric field component perpendicular to the metal surface is enhanced, SEIRA signals are not detectable for vibrations associated with dipole moment changes parallel to the surface. The enhancement is distinctly smaller than for SERS as only the field of the incident radiation is enhanced. However, for this reason the distance-dependence is not as steep because it scales only with the sixth power of the distance with respect to the centre of the island (Fig. 2.13).

$$F_{SEIRA}(d) = F_{SEIRA}(0) \cdot \left(\frac{a_0}{a_0 + d} \right)^6 \tag{2.81}$$

Even though enhancement factors are only between 10^2 and 10^3, the sensitivity gain of the SEIRA is large enough to apply this technique to biological molecules as the signals are detected in the difference mode (Ataka and Heberle 2003, 2004).

Box 2A

Quantum mechanical treatment of the harmonic oscillator

Transformation of the mass-weighted Cartesian coordinates q_i into normal coordinates Q_k is carried out such that $Q_k \cdot Q_{k'}$ cross terms are avoided in the expression for the kinetic and the potential energies [see Eq. (2.24)] (Wilson et al. 1995). Thus the kinetic energy T and the potential energy V are given by

$$T = \frac{1}{2} \sum_{k=1}^{3N-6} \dot{Q}_k^2 \tag{2.A1}$$

and

$$V = \frac{1}{2} \sum_{k=1}^{3N-6} \lambda_k Q_k^2 \tag{2.A2}$$

in analogy to Eqs. (2.15 and 2.17).

Hence, the Schrödinger equation

$$-\frac{h^2}{8\pi^2 m} \nabla^2 \psi + \hat{V} \psi = E \psi \tag{2.A3}$$

Box 2A *(continued)*

adopts the form

$$-\frac{h^2}{8\pi^2}\sum_{k=1}^{3N-6}\frac{\partial^2\psi_\nu}{\partial Q_k^2}+\frac{1}{2}\sum_{k=1}^{3N-6}\lambda_k\cdot Q_k^2\psi_\nu = E_\nu\psi_\nu \qquad (2.A4)$$

Solving this differential equation leads to the eigenvalues of the vibrational states given by

$$E_\nu = \left(v+\frac{1}{2}\right)h\nu_k \qquad (2.A5)$$

with the vibrational quantum number $v = 0, 1, 2\ldots$. The eigenfunctions of Eq. (2.A4) are expressed by

$$\psi_{v,k} = N_{v,k}\cdot H_{v,k}(Q_k)\cdot\exp\left(-\frac{1}{2}\gamma_k Q_k^2\right) \qquad (2.A6)$$

where $N_{v,k}$ is the normalisation constant

$$N_{v,k} = \left[\sqrt{\frac{\gamma_k}{\pi}}\cdot\frac{1}{2^v\cdot v!}\right]^{1/2} \qquad (2.A7)$$

The quantity γ_k is defined by

$$\gamma_k = \frac{4\cdot\pi^2\nu_k}{h} \qquad (2.A8)$$

$H_{v,k}$ denotes the Hermitian polynom, which varies with the vibrational quantum number v. Only for $v = 0$ is it equal to 1, whereas for $v \neq 0$ it becomes a function of Q_k (Atkins 2006). For $v = 1$, $H_{v,k}$ is equal to $H_{v,k} = \sqrt{\gamma_k}\cdot Q_k$ and the order of the polynom in terms of Q_k increases with increasing v. This corresponds to the increasing number of nodes of the wavefunction and thus affects its symmetry.

The vibrational wavefunctions actually have to be expressed as a product of the wavefunctions of the individual normal coordinates. However, the less exact treatment employed here for the sake of simplicity is appropriate to demonstrate the essential consequences for the IR, Raman, and resonance Raman selection rules (see also Box 2C). For a more thorough treatment the reader is referred to the literature (Herzberg 1945; Wilson et al. 1955).

Box 2B

Symmetry of molecules and vibrations

The symmetry of molecules is defined by a set of operations, which, when applied to the molecule, produce an identical copy (Cotton 1990). To illustrate these transformations we will consider the water molecule as a simple example (Fig. 2.B1). The three atoms of the molecule define a plane σ_{xz}, which is a symmetry plane; i.e., reflection at this plane leaves the molecule unchanged. A second plane of reflection σ_{xy} is perpendicular to σ_{xz} and bisects the bond angle. Furthermore, the intersection of both planes defines a rotational axis C_2. Upon rotation of the molecule around this axis by $2\pi/n$ ($n = 2$; two-fold axis). Other molecules may exhibit higher order rotational axes (e.g., a three-fold axis C_3 in the carbonate ion), a centre of inversion i (e.g., SF_6 with the sulfur atom being the centre of inversion), or a rotation–reflection plane S_n corresponding to the rotation around an n-fold axis and the subsequent reflection at the plane perpendicular to the rotational axis. The reflections σ, rotations C_n, rotation–reflections S_n, and the inversion I, in addition to the identity operation E which, just as a formal operation, leaves the molecule unchanged, constitute groups of symmetry operations that allows classification of all molecules into so-called point groups.

   The simplest situation, which holds for many biological molecules, is given if nothing other than the identity operation applies. These molecules, which lack any symmetry, belong to the point group C_1. Nevertheless, there are also molecular groups of biological interest of higher symmetry, or whose geometry can be approximated by a point group of higher symmetry. Our example H_2O, which possesses two mirror planes and a two-fold rotational axis, belongs to the point group C_{2v}. The properties
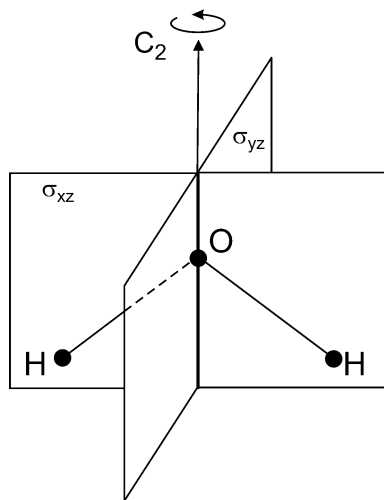

Fig. 2.B1 Symmetry operations of the C_{2v} point group, illustrated for the example of the water molecule. The two-fold rotational axis is denoted by C_2, the two mirror planes are indicated by σ_{xz} and σ_{yz}.

Box 2B *(continued)*

of these groups and the implications for (vibrational) spectroscopy become evident within the framework of group theory (Cotton 1990). Group theory by itself is a subject of pure mathematics, but it can be applied to many different fields of physics and physical chemistry. Therefore, all theorems used in the applications are based on formal derivations. Nevertheless, we consider it important to demonstrate the benefits of group theory by a more intuitive approach. Many aspects are taken from the book by Wilson, Decius and Cross, in which the application of group theory to vibrational spectroscopy is treated extensively (Wilson et al. 1955).

   All elements (all symmetry operations) of a point group can be represented by matrices according to

$$\begin{pmatrix} x' \\ y' \\ z' \end{pmatrix} = \begin{pmatrix} R_{11} & R_{12} & R_{13} \\ R_{21} & R_{22} & R_{23} \\ R_{31} & R_{32} & R_{33} \end{pmatrix} \begin{pmatrix} x \\ y \\ z \end{pmatrix} \tag{2.B1}$$

where R_{ij} constitute the elements of the transformation matrix that transform the coordinates of the molecule x, y, z into the coordinates x', y', and z'. These transformations can be illustrated by the reflection at the zy plane (Fig. 2.B2). Whereas the z- and y-coordinates remain unchanged, the x-coordinates just changes the sign such that $x' = x$. The transformation matrix is then given by
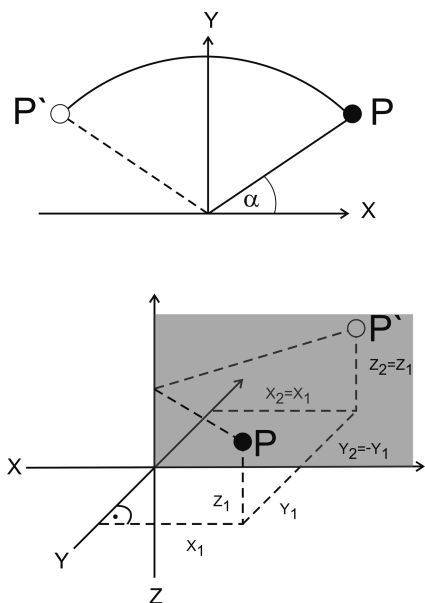

Fig. 2.B2 Transformation of P (solid circle) into P′ (open circle) by rotation around the *z*-axis (top) and by reflection through the *xz*-plane (bottom).

Box 2B *(continued)*

$$R(\sigma_{v,zy}) = \begin{pmatrix} -1 & 0 & 0 \\ 0 & 1 & 0 \\ 0 & 0 & 1 \end{pmatrix} \qquad (2.B2)$$

For an *n*-fold rotational axis perpendicular to the *yx*-plane (Fig. 2.B2) one obtains

$$z' = z$$

$$x' = x \cdot \cos(2\pi/n) - y \cdot \sin(2\pi/n) \qquad (2.B3)$$

$$y' = x \cdot \sin(2\pi/n) + y \cdot \cos(2\pi/n)$$

such that the transformation matrix yields

$$R(C_n) = \begin{pmatrix} \cos(2\pi/n) & -\sin(2\pi/n) & 0 \\ \sin(2\pi/n) & \cos(2\pi/n) & 0 \\ 0 & 0 & 1 \end{pmatrix} \qquad (2.B4)$$

These matrices describe the physical symmetry operations of the molecule.

As molecular vibrations involve distortions of the geometry, it is interesting to ask how such distortions transform under the symmetry operations of the molecule. We will take as an example the nitrate molecule, consisting of three oxygen atoms and one nitrogen atom. The symmetry is the D_{3h} point group (one 3-fold rotational axis, one horizontal mirror plane, three vertical mirror planes, three two-fold rotational axes, and the alternating 3-fold rotational axis obtained from the combination of the normal three-fold axis with the horizontal mirror plane). The deformation of the molecule is denoted by q_i with *i* running from 1 to $3N$ (for nitrate it runs from 1 to 12). The transformed displacements q_j' can be obtained for each symmetry operation by the linear equations

$$q_j' = \sum_{i=1}^{3N} R_{ji} q_i \qquad (2.B5)$$

Of course, the matrices R_{ji} defined here are different from the 3×3 matrices (2.B1) describing the physical symmetry operations of the corresponding point group, although they are closely related. They are "isomorphic" to each other. The $3N \times 3N$ matrices R_{ji} (2.B5) are known as a representation of the point group, and the displacements q_i are termed the basis of this representation.

It can be shown that the matrix (2.B5) can be greatly simplified by a particular transformation of the coordinate system according to

$$\eta_i = \sum_{j}^{3N} \alpha_{ij} q_j \qquad (2.B6)$$

Box 2B *(continued)*

Then the matrix (2.B5) transforms into

$$R'_{i'j'} = \sum_{ij}^{3N} \alpha_{i'i} R_{ij} (\alpha^{-1})_{jj'} \tag{2.B7}$$

where α^{-1} denotes the reciprocal of the transformation (2.B6).

For each symmetry operation R of a point group a transformation α_{ij} can be found such that the transformed operation R contains only diagonal elements

$$\eta'_i = R'_{ii} \eta_i \tag{2.B8}$$

It is generally not possible to find a single transformation by which all operations of a point group are converted into diagonal forms. However, as general derivations in group theory show, there are transformations that simplify the matrices of all the symmetry operations of a point group considerably. If the cubic groups are excluded, the corresponding matrices consist of diagonal elements and of blocks of 2×2 matrices such as:

$$\begin{pmatrix} R_{11} & & & & & & \\ & R_{22} & R_{23} & & & & \\ & R_{32} & R_{33} & & & & \\ & & & R_{3N-2,3N-2} & R_{3N-2,3N-1} & & \\ & & & R_{3N-1,3N-2} & R_{3n-1,3N-1} & & \\ & & & & & & R_{3N3N} \end{pmatrix} \tag{2.B9}$$

For the cubic groups there are also blocks of 3×3, 4×4, and 5×5 matrices. It is evident that there are different matrix representations determined by the transformation (2.B6). It is straightforward to show that what all these representations have in common is that the trace of the matrices is the same, i.e.,

$$\sum_{i}^{3N} R'_{ii} = \sum_{i}^{3N} R_{ii} = \chi_R \tag{2.B10}$$

This trace χ_R is called the character of the symmetry operation R.

Thus, in all these representations the symmetry operations are characterised by the unique value of the traces of the matrices representing the corresponding operations. If a representation is found such that all the matrices are of the form in Eq. (2.B9), the representation is referred to as being completely reduced. The corresponding new basis has the property that it can be separated into sets that do not mix with each other upon the various symmetry operations of this point group. Therefore, the transformation equations for the members of each set of the new basis can, by themselves, be

Box 2B *(continued)*

regarded as a representation of the point group. As no transformation can further simplify (reduce) the representation, it is termed an irreducible representation. Therefore, a completely reduced representation as given by the matrices such as in Eq. (2.B9) is made up of a number of irreducible representations and the character of the completely reduced representation (or of the reducible representation) is the sum of the characters of the irreducible representations, i.e.,

$$\chi_R = \sum_\gamma n^{(\gamma)} \chi_R^{(\gamma)} \qquad (2.B11)$$

where χ_R^γ is the character of the irreducible representation γ with respect to the symmetry operation R, and $n^{(\gamma)}$ specifies how often the representation γ appears in the completely reduced representation. It can be shown that

$$n^{(\gamma)} = \frac{1}{g} \sum_R \chi_R^\gamma \chi_R \qquad (2.B12)$$

where the sum extends over all symmetry operations of a point group and g gives the number of symmetry operations.

An additional nomenclature has to be introduced. There are symmetry operations that have the same various characters for the different irreducible representations. These operations belong to the same class. A more formal definition for a class is the following: if A, B, and X are members of a point group and if $B = X^{-1}AX$, then A and B belong to the same class. It is easy to show that the equality of the characters of A and B follows from the definition of character and from the rule of matrix multiplication. In characterising a point group, it is, therefore, not necessary to give the characters of all symmetry operations but it is sufficient to list them for each different class of symmetry operations.

Using the classes of symmetry operations, Eq. (2.B12) can be rewritten as

$$n^{(\gamma)} = \frac{1}{g} \sum_j g_j \chi_j^{(\gamma)} \chi_j \qquad (2.B13)$$

where g_j is the number of elements (symmetry operations) within the class j, $\chi_j^{(\gamma)}$ is the character of the representation γ with respect to the class j, and χ_j is the character of any one of the symmetry operations within class j with respect to the completely reduced or reducible representation (as has been shown above, the character of a symmetry operation is not changed by a transformation of the coordinate system).

The representation of a point group is characterised by the character of the transformations making up this point group. Therefore, the transformation properties of the irreducible representations, i.e., the characters, can be summarised in tabular form. They are listed for the different point groups in books describing the application

Box 2B *(continued)*

of group theory (e.g., Wilson et al. 1955). For the D_{3h} point group, the character table is

D_{3h}	E	$2C_3$	$3C_2$	σ_h	$2S_3$	$3\sigma_v$	
A_1'	1	1	1	1	1	1	
A_2'	1	1	−1	1	1	−1	
E'	2	−1	0	2	−1	0	(2.B14)
A_1''	1	1	1	−1	−1	−1	
A_2''	1	1	−1	−1	−1	1	
E''	2	−1	0	−2	1	0	

The symbol in the upper left corner denotes the point group. The first column contains the various irreducible representations, in this case 6. The first row lists the various symmetry operations (unity operation E, two rotations about the 3-fold axis, one horizontal mirror plane σ_h, two alternating rotations about the 3-fold axis, and three vertical mirror planes σ_v). The second column, describing the characters of the unity operation E for the various irreducible representations, gives the dimensionality of the representation, i.e., the number of coordinates that may mix upon application of the symmetry operations. The notation for the different representations is complex (Mullican notation) and basically describes the symmetry properties upon certain basic symmetry operations of the different point groups. Here, it is sufficient to note that the letters A and B refer to one-dimensional representations, the letters E and F to two-dimensional and three-dimensional representations. Typically not all symmetry operations are listed, rather the classes together with the number of operations within the particular class.

It is easy to see that for the D_{3h} symmetry we obtain $n(A_1') = 1$; $n(A_2'') = 2$; $n(E') = 3$; $n(E'') = 1$; $n(A_2') = 1$. It is important to mention that the D_{3h} representation of the displacements as the basis does not contain the A_1'' irreducible representation.

What is the connection for these symmetry considerations with vibrational spectroscopy? It has been shown in Section 2.1.1 that the normal coordinates Q_i involve a linear transformation such as (2.B6)

$$Q_k = \sum l_{ik} q_i \qquad (2.B15)$$

It is straightforward to show that these normal coordinates form part of the irreducible representations making up the basis set of the displacements (see Wilson et al. 1955). In general, there are 6 additional representations, 3 for the translational and 3 for the rotational movements of the molecule as a whole. Thus, the normal coordinates Q_i just transform as irreducible representations, and their symmetry properties are given by the character table.

Box 2B *(continued)*

We now can further specify the Mullican notation as given in the character tables, for the C_{2v} geometry of water [Eq. (2.B16)] or for the D_{3h} symmetry of nitrate [Eq. (2.B14)]. As already mentioned the letters A and B refer to one-dimensional, E to two-dimensional, and F to three-dimensional representations. Totally symmetric representations for which all characters are 1 are denoted by A, A_1, or A_{1g}. The subscript "*g*" is the abbreviation for "gerade" indicating the symmetry with respect to inversion whereas "ungerade" representations (denoted by the subscript "*u*") are antisymmetric toward this symmetry operation.

C_{2v}	E	C_2	$\sigma_v(xz)$	$\sigma_v(yz)$	
A_1	1	1	1	1	(2.B16)
A_2	1	1	−1	−1	
B_1	1	−1	1	−1	
B_2	1	−1	−1	1	

As an example, we can now discuss the symmetry properties for the normal modes of H_2O. The three normal modes are schematically represented in Fig. 2.B3. The stretching and bending modes ν_1 and ν_2 are symmetric (character $+1$) with respect to all symmetry operations, i.e., the rotation and the two reflections, and thus belong to the (totally symmetric) representation A_1 [Eq. (2.B16)]. The stretching mode ν_3, however, is anti-symmetric (character -1) to the rotation and the reflection with respect to the *yz*-plane, such that it is grouped into the B_1 representation.

Such a classification of the normal modes according to the symmetry properties can also be obtained by transforming internal coordinates into symmetry coordinates. For the water molecule, this transformation is relatively simple assuming an approximate expression for the potential energy

$$2V = F_r(r_1^2 + r_2^2) + F_\alpha \alpha^2 \tag{2.B17}$$

where $r_1(r_2)$ and α are the stretching and bending coordinates, respectively. F_r and F_α denote the corresponding stretching and bending force constants, whereas interaction force constants are neglected. If we now define symmetry coordinates according to
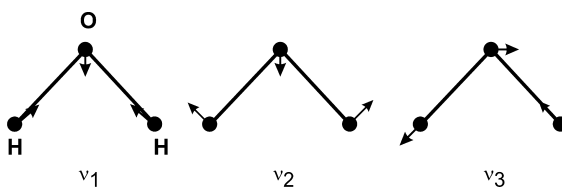

Fig. 2.B3 Illustration of the three normal modes of water. The arrows qualitatively indicate the directions of displacements of the individual atoms in the normal modes.

Box 2B *(continued)*

$$S_1 = \alpha$$

$$S_2 = \frac{1}{\sqrt{2}}(r_1 + r_2) \tag{2.B18}$$

$$S_2 = \frac{1}{\sqrt{2}}(r_1 - r_2)$$

the potential energy [Eq. (2.B6)] is then expressed by

$$2V = F_\alpha S_1^2 + F_r S_2^2 + F_r S_3^2 \tag{2.B19}$$

Correspondingly, the kinetic energy is given in terms of these symmetry coordinates

$$2T = M_\alpha \dot{S}_1^2 + 2\sqrt{2} M_{\alpha r} \dot{S}_1 \dot{S}_2 + (M_{rr} + M_r)\dot{S}_2^2 + (M_r - M_{rr})\dot{S}_3^2 \tag{2.B20}$$

where M_i are the reduced masses which constitute the inverse G-matrix.

With Eqs. (2.B19 and 2.B20) one obtains the secular equation

$$\begin{vmatrix} F_\alpha - M_\alpha \lambda & -\sqrt{2} M_{\alpha r}\lambda & 0 \\ -\sqrt{2} M_{\alpha r}\lambda & F_r - (M_r + M_{rr})\lambda & 0 \\ 0 & 0 & F_r - (M_r - M_{rr})\lambda \end{vmatrix} = 0 \tag{2.B21}$$

which factorises into two blocks, a 2×2 matrix referring to the normal modes of the A_1 representation, and a 1×1 matrix corresponding to the B_1 mode.

An important goal of group theory applied to molecular vibrations is to determine the number of normal modes n belonging to each irreducible representation γ of the point group. This procedure, which substantially facilitates the assignment of Raman and infrared bands (*vide infra*), can be applied on the basis of Cartesian (displacement) coordinates or internal (symmetry) coordinates. We have mentioned above that the number of given irreducible representations appears in the completely reduced representation according to Eq. (2.B13), i.e.,

$$n^{(\gamma)} = \frac{1}{g}\sum_j g_j \chi_j^{(\gamma)} \chi_j \tag{2.B13}$$

This expression can be used to determine the number of normal modes in a certain irreducible representation γ, taking into account that expressions (2.B13) also contain the 6 coordinates for translation and rotation. g_j and $\chi_j^{(\gamma)}$ are obtained from the character tables such as Eqs. (2.B14 and 2.B16). χ_j has to be determined independently, either by inspection of the effects of the symmetry operations on the displacement coordinates, or by more efficient methods described in books on the application of group theory.

Box 2B *(continued)*

Let us consider the situation when the molecular vibrations are described in terms of Cartesian displacement coordinates. It is clear that for a 3-atomic molecule χ_E equals 9 ($3N$). For a three-atomic molecule such as H_2O, the values of χ_j are determined to be -1, 3, and 1 for the symmetry operations C_2, $\sigma_{v,xz}$, and $\sigma_{v,yz}$, respectively. With Eq. (2.B13) we obtain

$$n(A_1) = \frac{1}{4}(1 \cdot 1 \cdot 9 - 1 \cdot 1 \cdot 1 + 1 \cdot 1 \cdot 3 + 1 \cdot 1 \cdot 1) = 3$$

$$n(A_2) = \frac{1}{4}(1 \cdot 1 \cdot 9 - 1 \cdot 1 \cdot 1 - 1 \cdot 1 \cdot 3 - 1 \cdot 1 \cdot 1) = 1$$

$$n(B_1) = \frac{1}{4}(1 \cdot 1 \cdot 9 + 1 \cdot 1 \cdot 1 + 1 \cdot 1 \cdot 3 - 1 \cdot 1 \cdot 1) = 3 \qquad (2.B22)$$

$$n(B_2) = \frac{1}{4}(1 \cdot 1 \cdot 9 + 1 \cdot 1 \cdot 1 - 1 \cdot 1 \cdot 3 + 1 \cdot 1 \cdot 1) = 2$$

which can be summarised by

$$\Gamma = 3A_1 + A_2 + 3B_1 + 2B_2 \qquad (2.B23)$$

Thus, altogether we have 9 modes corresponding to the $3N = 9$ degrees of freedom. To sort out the ''modes'' of zero frequency, we have to consider the symmetry properties of the translational and rotational degrees of freedom. Translation of the molecule in *z*-direction (T_z) is symmetric with respect to all symmetry operations such that T_z is assigned to the A_1 symmetry species. Translation in the *x*- and *y*-directions is symmetric with respect to $\sigma_{v,xz}$ and $\sigma_{v,yz}$, respectively, but both are antisymmetric with respect to C_2. Thus, T_x and T_y belong to the symmetry species B_1 and B_2, respectively. Correspondingly, one can show that rotation around the *z*-axis R_z is symmetric with respect to C_2 but antisymmetric with respect to both reflections. Likewise, we find that R_x and R_y are antisymmetric to C_2 but symmetric to $\sigma_{v,zx}$ and $\sigma_{v,zy}$, respectively, such that for these molecular motions the assignment to the symmetry species is also straightforward. Thus, we subtract the translations and rotations from the respective symmetry species to obtain the true number of vibrational normal modes. This approach is readily applicable to larger molecules and, moreover, it also holds for the internal co-ordinate system. In this way, it is possible to factorise the *FG*-matrix into blocks corresponding to the various symmetry species involved. The translational (T_x, T_y, T_z) and rotational (R_x, R_y, R_z) coordinates are usually included into the character table, so one obtains for the C_{2v} symmetry.

Box 2B *(continued)*

C_{2v}	E	C_2	$\sigma(xz)$	$\sigma(yz)$	
A_1	1	1	1	1	T_z
A_2	1	1	−1	−1	R_z
B_1	1	−1	1	−1	T_x; R_y
B_2	1	−1	−1	1	T_y; R_x

(2.B24)

For the real normal modes we obtain Γ(normal modes) $= 2A_1 + B_1$, as intuitively derived for this simple molecule.

Box 2C

Symmetry-based selection rules

Symmetry considerations allow the determination of whether a normal mode Q_k of a molecule belonging to a certain point group ($\neq C_1$) is IR- or Raman-active. This establishes if the expressions for the transition dipole moment [Eq. (2.44)] and the scattering tensor [Eq. (2.62)] are zero or non-zero. In symmetry terms this means: the product, in which $\hat{\Omega}$ is the dipole moment or polarisability operator, must lead to a symmetric function otherwise the integrals in Eqs. (2.44 and 2.62) vanish. Within the framework of group theory (Cotton 1990; Wilson et al. 1955), the symmetry properties of this product are expressed by the ''direct product'' of the irreducible representations

$$\Gamma = \Gamma_n \times \Gamma_\Omega \times \Gamma_m \qquad (2.C1)$$

where Γ_n, Γ_m, and Γ_Ω are the irreducible representations of the wavefunctions of the initial, and the final states, and of the operator, respectively. The condition that the integral over the products in Eqs. (2.44 and 2.62) is non-zero requires that the direct product has the totally symmetric irreducible representation.

Let us first consider the wavefunction of the vibrational ground state $\psi_{n,k}$ ($v = 0$), which we can express by the symmetric eigenfunction of the harmonic oscillator (see Box 2A)

$$\psi_{n,k} = N_{0,k} \cdot \exp\left(-\frac{1}{2}\gamma_k Q_k^2\right) \qquad (2.C2)$$

which is always totally symmetric. The actual ground state is the product of such functions belonging to the various normal modes. However, because in a fundamental vibrational transition only one normal mode is involved, it is sufficient to consider only the expression Eq. (2.C2). The situation is different if a transition to a combination state has to be treated.

For the first vibrational excited state ψ_m ($v = 1$), however, the eigenfunction is given by

Box 2C *(continued)*

$$\psi_{m,k} = N_{1,k} \cdot \sqrt{\gamma_k} \cdot Q_k \cdot \exp\left(-\frac{1}{2}\gamma_k Q_k^2\right) \tag{2.C3}$$

such that the symmetry of $\psi_{m,k}$ is given by the symmetry of Q_k.

Now we can investigate the consequences for the IR transitions. In this instance, the operator $\hat{\Omega}$ corresponds to the dipole moment operator [Eq. (2.44)], which has three components corresponding to the Cartesian coordinates

$$\mu_x = \sum_\alpha e_\alpha \cdot x_\alpha$$

$$\mu_y = \sum_\alpha e_\alpha \cdot y_\alpha \tag{2.C4}$$

$$\mu_z = \sum_\alpha e_\alpha \cdot z_\alpha$$

Evidently, the operator $\hat{\mu}$ transforms in the same manner as the Cartesian coordinates or as the translations in the *x*-, *y*-, and *z*-directions. Thus, the irreducible representations of μ_i, i.e., Γ_μ, can be derived from the character table of the individual point groups.

To determine the symmetry product according to Eq. (2.C1), we use the multiplication properties of the irreducible representations (Wilson et al. 1955). For the non-degenerate species A and B, these rules are fairly simple as $A \times A = A$ and $B \times B = A$, whereas $A \times B = B$. Likewise, for the subscripts we have $1 \times 1 = 1$, $2 \times 2 = 1$ and $1 \times 2 = 2$ (except for D_2 and D_{2h} point groups) and $g \times g = g$, $u \times u = g$ and $g \times u = u$. On this basis, we can decide which of the vibrational modes of H_2O are IR-active. For the two A_1 modes, with Eq. (2.C1) we obtain

$$\Gamma_{A_1}(z) = A_1 \times A_1 \times A_1 = A_1$$

$$\Gamma_{A_1}(y) = A_1 \times B_2 \times A_1 = B_2 \tag{2.C5}$$

$$\Gamma_{A_1}(x) = A_1 \times B_1 \times A_1 = B_1$$

implying that both A_1 modes are IR-active but only the *z*-component of the dipole moment operator provides a non-zero contribution to the transition dipole moment. Correspondingly, one obtains for the B_1 mode

$$\Gamma_{B_1}(z) = A_1 \times A_1 \times B_1 = B_1$$

$$\Gamma_{B_1}(y) = A_1 \times B_2 \times B_1 = A_2 \tag{2.C6}$$

$$\Gamma_{A_1}(x) = A_1 \times B_1 \times B_1 = A_1$$

Thus, in this instance only the *x*-component of $\hat{\mu}$ gives rise to the IR intensity.

Although the direct product formalism is general and in particular allows the treatment of more complex transitions involving overtones and combinational levels, for the fundamental transition there is an even simpler rule, which can be readily obtained.

It can be shown that the character of the direct product of two irreducible representations is the product of their characters. The condition that

Box 2C *(continued)*

$$\Gamma = \Gamma_n \times \Gamma_\Omega \times \Gamma_m \qquad\qquad (2.C1)$$

contains the totally symmetric representation can be rephrased to ask how many times this representation is contained in Γ. According to Eq. (2.B12), this value, $n^{(1)}$, is given by

$$n^{(1)} = \frac{1}{g} \sum_R \chi_R^n (\chi_R^\Omega \chi_R^m) \qquad\qquad (2.C7)$$

as the character of the totally symmetric representation, $\chi_R^{(1)}$, equals one for all operations R. Expression (2.C7) can be considered in such a way that $n^{(1)}$ represents the number of times Γ_n is contained in the reducible representation $\Gamma_\Omega \times \Gamma_m$.

Therefore, if Γ_n does occur, $n^{(1)}$ is greater than zero and the integral does not vanish. For the fundamental transition from the ground state (totally symmetric) to the first excited vibronic level, one therefore arrives at the very simple statement that such a transition is IR active if the corresponding normal coordinate belongs to the same representations as those of T_x, T_y, or T_z.

In the same way we determine the Raman activity on the basis of the symmetry properties of the operator for the polarisability tensor, Eq. (2.62). It can be shown (Wilson et al. 1955) that the components of this operator $\hat{\alpha}_{xx}$, $\hat{\alpha}_{xy}$, $\hat{\alpha}_{xz}$ etc. transform as do *xx*, *xy*, *xz* etc. Therefore, the transformation properties of the tensor can be derived in a similar way as for the *x*-, *y*-, and *z*-coordinates themselves. These symmetry properties are also listed in the character table, and Eq. (2.B24) is extended to

C_{2v}	E	C_2	$\sigma_v(xz)$	$\sigma_v(yz)$			
A_1	1	1	1	1	T_z	$\alpha_{xx};\ \alpha_{yy};\ \alpha_{zz}$	(2.C8)
A_2	1	1	-1	-1	R_z	α_{xy}	
B_1	1	-1	1	-1	$T_x;\ R_y$	α_{xz}	
B_2	1	-1	-1	1	$T_y;\ R_x$	α_{yz}	

As shown in Chapter 2, the Raman scattering involves a change in the quantum number of a normal mode by 1, as in the infrared absorption. Therefore, the same methodology as for infrared absorption can be applied. Either the general direct product formalism can be used, or one can determine whether an element of the polarisability operator belongs to the same representation as a normal mode. We readily find that the A_1 modes are Raman-active through the tensor components α_{xx}, α_{yy}, and α_{zz}, whereas the B_1 mode gains Raman intensity through α_{xz}. By means of Eqs. (2.60 and 2.61), we can conclude that the A_1 modes exhibit a very small depolarisation ratio whereas this ratio is 0.75 for the B_1 mode. Thus, symmetry consideration do not only allow prediction for the Raman- and IR-activity of the normal modes but also provides predictions for the depolarisation ratio, which in turn is particularly helpful for the vibrational assignments.

Box 2C *(continued)*

Now we consider the RR activity. For the *A*-term [Eq. (2.68)], the RR intensity depends on the electronic transition dipole moments M_{GR}^0 and the Franck–Condon factor products $\langle nr \rangle \langle rm \rangle$. As the vibrational quantum number for the initial and final wavefunctions differs by one, either the left or the right integral would vanish for non-totally symmetric modes. Thus, only totally-symmetric modes gain intensity via the *A*-term, given that the origins of the potential curves in the ground and electronic excited state are displaced with respect to each other. The second prerequisite for *A*-term RR intensity is defined by the symmetry properties of M_{GR}^0

$$\Gamma = \Gamma_G \times \Gamma_\Omega \times \Gamma_R \tag{2.C9}$$

where the irreducible representation of the dipole moment operator Γ_Ω corresponds to that of the transition dipole moment as in the case of IR absorption [Eq. (2.C4)]. The electronic transition moment is non-zero if there is a component (in the *x*-, *y*-, or *z*-direction) for which the direct product Eq. (2.C9) is totally symmetric.

As an example, we will discuss the $\pi \to \pi^*$ electronic transitions of benzene, which belongs to the D_{6h} point group. The electronic configuration can be illustrated within the Hückel approximation of molecular orbital theory (Fig. 2.C1). In the electronic ground state, the three occupied π-orbitals are of a_{2u} and e_{1g} symmetry, leading to the $(a_{2u})^2(e_{1g})^4$ configuration. As all occupied orbitals are completely filled, the
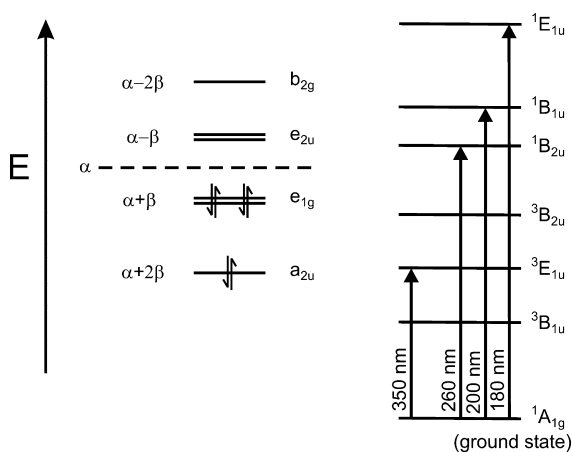

Fig. 2.C1 Electronic structure (left) and energy diagram for the electronic transitions (right) of benzene (Straughan and Walker 1976). The electronic structure is qualitatively described in terms of the Hückel molecular orbital approximation.

Box 2C *(continued)*

ground state belongs to the totally symmetric species $^1A_{1g}$ where the superscript "1" indicates the singlet state. The lowest electronic excitation promotes an electron to the e_{2u} orbital resulting in the $(a_{2u})^2(e_{1g})^3(e_{2u})^1$ configuration (Fig. 2.C1). The direct product of (e_{1g}) and (e_{2u}) then leads to symmetry properties of the three lowest excited states, i.e., $^1B_{1u}$, $^1B_{2u}$, and $^1E_{1u}$ (considering only the singlet transitions). Thus, the irreducible representation of the corresponding electronic transition dipole moments are evaluated according to Eq. (2.C9) using the irreducible representations of the dipole moment operator that are A_{2u} (z) and E_{1u} (x, y) within the D_{6h} point group. It can be verified that only the product $A_{1g} \times E_{1u} \times E_{1u}$ leads to a totally symmetric species implying that only the $^1E_{1u} \leftarrow {}^1A_{1g}$ transition, which is localised in the x, y-plane, is symmetry-allowed. This transition in fact gives rise to a strong absorption band at ca. 180 nm and excitation in resonance with this transitions provides a strong enhancement of the Raman bands originating from totally-symmetric A_{1g} modes.

Now we will consider the symmetry-based selection rules for the *B*-term scattering mechanism. When the excitation is in resonance with a weak electronically excited state *R*, the Herzberg–Teller approximation (Albrecht 1961) applies and Eq. (2.69) is transformed into

$$B \cong \frac{1}{h} \frac{M_{GS}^0 M_{GR}^0 H_{RS}}{v_S - v_R} \sum_r \left(\frac{\langle n|Q_k|r\rangle\langle rm\rangle + \langle n|r\rangle\langle r|Q_k|m\rangle}{v_{Rr} - v_k - v_0 + i\Gamma_R} \right) \tag{2.C10}$$

where H_{RS} is the vibronic coupling integral describing the mixing between the resonant excited state *R* and a second (allowed) excited state *S*, and v_S and v_R are the frequencies of the corresponding $0 \rightarrow 0$ excitations.

Again, we restrict the discussion to the transition from the vibrational ground state *n* (with $v = 0$) to the first vibrational excited state *m* (with $v = 1$), and inspect the individual terms in Eq. (2.C10) separately. The vibrational integrals that include the normal coordinate Q_k, i.e., $\langle n|Q_k|r\rangle$ and $\langle r|Q_k|m\rangle$, are only non-zero if the symmetry product of Q_k with $\psi_{m,k}$ or $\psi_{r,k}$ is totally-symmetric. In addition, the integrals $\langle n|r\rangle$ and $\langle r|m\rangle$ must be non-zero, which is only fulfilled for $\psi_{r,k}$ having the same vibrational quantum number as $\psi_{n,k}$ or $\psi_{m,k}$. Finally, the integral H_{RS} has to be large, which is true for modes that can effectively couple the electronically excited states *R* and *S*. Combining these three conditions, maximum enhancement via the *B*-term mechanism is expected:

(i) for modes of the symmetry species given by the direct product of the two electronic transitions that are involved

(ii) when the excitation line is in resonance with the weak $0 \rightarrow 0$ or $0 \rightarrow 1$ vibronic transition *Rr*

(iii) when the energy difference with respect to a second electronically excited state *S* is small.

References

Albrecht, A. C., **1961**, ''On the theory of Raman intensities'', *J. Chem. Phys.* **34**, 1476–1484.

Albrecht, A. C., Hutley, M. C., **1971**, ''On the dependence of vibrational Raman intensity on the wavelength of incident light'', *J. Chem. Phys.* **55**, 4438–4443.

Ataka, K., Heberle, J., **2003**, ''Electrochemically induced surface-enhanced infrared difference absorption (SEIDA) spectroscopy of a protein mono-layer'', *J. Am. Chem. Soc.* **125**, 4986–4987.

Ataka, K., Heberle, J., **2004**, ''Functional vibrational spectroscopy of a cytochrome *c* monolayer: SEIDAS probes the interaction with different surface-modified electrodes'', *J. Am. Chem. Soc.* **126**, 9445–9457.

Atkins, P., **2006**, ''*Physical Chemistry*'', Oxford University Press, Oxford.

Blair, D. F., Campbell, G. W., Schoonover, J. R., Chan, S. I., Gray, H. B., Malmström, B. G., Pecht, I., Swanson, B. I., Woodruff, W. H., Ch., W. K., English, A. M., Fry, H. A., Lunn, V., Norton, K. A., **1985**, ''Resonance Raman studies of blue copper proteins: Effect of temperature and isotope substitutions. Structural and thermo-dynamic implications'', *J. Am. Chem. Soc.* **107**, 5755–5766.

Cotton, F. A., **1990**, ''*Chemical Applications of Group Theory*'', Wiley, New York.

Curry, B., Palings, I., Broek, A. D., Pardoen, J. A., Lugtenburg, J., Mathies, R., **1985**, ''Vibrational analysis of the retinal isomers'', in *Adv. Infrared and Raman Spectrosc.* **12**, Clark, R. J. H., Hester, R. E. (Eds.), chap. 3, Wiley, Heyden, New York.

Czernuszewicz, R. S., Spiro, T. G., **1999**, ''IR, Raman, and resonance Raman spectroscopy'', in *Inorganic Electronic Structure and Spectroscopy*, Solomon, E. I., Lever, A. B. P. (Eds.), Vol. 1, Wiley, New York, pp. 353–441.

Fogarasi, G., Zhou, X., Taylor, P. W., Pulay, P., **1992**, ''The calculation of *ab-initio* molecular geometries: Efficient optimiza-tion by natural internal coordinates and empirical corrections of offset forces'', *J. Am. Chem. Soc.* **114**, 8191–8201.

Heller, E. J., **1981**, ''The semi-classical way to molecular spectroscopy'', *Acc. Chem. Res.* **14**, 368–375.

Herzberg, G., **1945**, ''*Molecular Spectra and Molecular Structure: II, Infrared and Raman Spectra of Polyatomic Molecules*'', Van Nostrand Reinhold, New York.

Hildebrandt, P., Stockburger, M., **1984**, ''Surface enhanced resonance Raman spectroscopy of Rhodamine 6G adsorbed on colloidal silver'', *J. Phys. Chem.* **88**, 5935–5944.

Kerker, M., Wang, D. S., Chew, S., **1980**, ''Surface enhanced Raman scattering (SERS) by molecules adsorbed on spherical particles'', *Appl. Opt.* **19**, 4159–4273.

Kneipp, K., Moskovits, M., Kneipp, H. (Eds.), **2006**, ''Surface-enhanced Raman scattering: Physics and applications'', *Topics Appl. Phys.* **103**, Springer, Berlin.

Li, X.-Y., Czernuszewicz, R. S., Kincaid, J. R., Spiro, T. G., **1989**, ''Consistent porphyrin force field. 3. Out-of-plane modes in the resonance Raman spectra of planar and ruffled nickel octaethylporphyrin'', *J. Am. Chem. Soc.* **111**, 7012–7023.

Li, X.-Y., Czernuszewicz, R. S., Kincaid, J. R., Su, Y. O., Spiro, T. G., **1990a**, ''Consistent porphyrin force field. 1. Normal mode analysis for nickel porphine and nickel tetraphenylporphine from resonance Raman and infrared spectra and isotope shifts'', *J. Phys. Chem.* **94**, 31–47.

Li, X.-Y., Czernuszewicz, R. S., Kincaid, J. R., Stein, P., Spiro, T. G., **1990b**, ''Consistent porphyrin force field. 2. Nickel octaethyl-porphyrin skeletal and substituent mode assignments from ^{15}N, meso-d_4, and methylene-d_{16} Raman and infrared isotope shifts'', *J. Phys. Chem.* **94**, 47–61.

Magdó, I., Nemeth, K., Mark, F., Hildebrandt, P., Schaffner, K., **1999**, ''Calculation of vibrational spectra of linear tetrapyrroles. Global sets of scaling factors for force fields derived by *ab-initio* and density functional theory methods'', *J. Phys. Chem. A* **103**, 289–303.

Mie, G., **1908**, ''Beiträge zur Optik trüber Medien, speziell kolloidaler Metallösun-gen'', *Ann. Physik* **25**, 377–445.

Moskovits, M., **1985**, ''Surface-enhanced spectroscopy'', *Rev. Mod. Phys.* **57**, 783–826.

Mroginski, M. A., Hildebrandt, P., Kneip, C., Mark, F., **2003**, ''Excited state geometry calculations and the resonance Raman

spectrum of hexamethylpyrromethene'', *J. Mol. Struct.* **661**–**662**, 611–624.

Mroginski, M. A., Németh, K., Bauschlicher, T., Klotzbücher, W., Goddard, R., Heinemann, O., Hildebrandt, P., Mark, F., **2005**, ''Calculation of vibrational spectra of linear tetrapyrroles. 3. Hydrogen bonded hexamethylpyrromethene dimers'', *J. Phys. Chem. A* **109**, 2139–2150.

Murgida, D. H., Hildebrandt, P., **2004**, ''Electron transfer processes of cytochrome *c* at interfaces. New insights by surface-enhanced resonance Raman spectroscopy'', *Acc. Chem. Res.* **37**, 854–861.

Murgida, D. H., Hildebrandt, P., **2005**, ''Redox and redox-coupled processes of heme proteins and enzymes at electrochemical interfaces'', *Phys. Chem. Chem. Phys.* **7**, 3773–3784.

Osawa, M., **1997**, ''Dynamic processes in electrochemical reactions studied by surface-enhanced infrared absorption spectroscopy (SEIRAS)'', *Bull. Chem. Soc. Jpn.* **70**, 2861–2880.

Otto, A., **2001**, ''Theory of first layer and single molecule surface enhanced Raman scattering (SERS)'', *Phys. Stat. Sol. A* **188**, 1455–1470.

Peticolas, W. L., Rush, T., **1995**, ''Ab-initio calculation of the ultraviolet resonance Raman spectra of Uracile'', *J. Comp. Chem.* **16**, 1261–1270.

Placzek, G., **1934**, ''Rayleigh-Streuung und Raman-Effekt'', in *Handbuch der Radiologie*, Vol. VI, Marx, E. (Ed.), chap. 3, Akademische Verlagsanstalt, Leipzig.

Rauhut, G., Pulay, P., **1995**, ''Transferable scaling factors for density functional derived vibrational force fields'' *J. Phys. Chem.* **99**, 3093–3100.

Straughan, B. P., Walker, S. (Eds.), **1976**, ''*Spectroscopy*'', Chapman and Hall, London.

Warshel, A., Dauber, P., **1977**, ''Calculations of resonance Raman spectra of conjugated molecules'', *J. Chem. Phys.* **66**, 5477–5488.

Wilson, E. B., Decius, J. C., Cross, P. C., **1955**, ''*Molecular Vibrations: The Theory of Infrared and Raman Vibrational Spectra*'', McGraw-Hill, New York.